Research Square

Preprints are preliminary reports that have not undergone peer review.
They should not be considered conclusive, used to inform clinical practice,
or referenced by the media as validated information.

Multi-omics Analysis Reveals the Molecular Basis of Antioxidant Activity in the Green Fruits of Rubus chingii Hu

Xiurong Xu
Zhejiang Academy of Forestry
Shiming Cheng
864569485@qq.com

Zhejiang Academy of Forestry

Article

Keywords: multi-omics analysis, molecular basis, Rubus chingii, green fruits, antioxidant activity

Posted Date: November 23rd, 2026

DOI: https://doi.org/10.21203/rs.3.rs-11329600/v1

License: This work is licensed under a Creative Commons Attribution 4.0 International License.
Read Full License

Additional Declarations: No competing interests reported.

Multi-omics Analysis Reveals the Molecular Basis of Antioxidant Activity in the Green Fruits of *Rubus chingii* Hu

Xiurong Xu[1], Shiming Cheng[1*]

Zhejiang Academy of Forestry, Hangzhou 310023, China

Corresponding author: Shiming Cheng；864569485@qq.com

Keywords: multi-omics analysis; molecular basis; *Rubus chingii*; green fruits; antioxidant activity

Abstract

Abstract: Green fruits of *Rubus chingii* Hu, listed as a "New Eight Zhejiang Authentic Herb", possess strong antioxidant activity, yet the underlying metabolites and regulatory mechanisms remain unclear. Here, physiological assays revealed significantly higher total phenolic content and ABTS/DPPH/FRAP antioxidant capacities in green fruits compared to other developmental stages, with highly significant positive correlations. Integrated metabolomics and weighted metabolite co-expression network analysis (WMCNA) identified 90 key antioxidant polyphenols (mainly flavonoids and phenolic acids). Network pharmacology and molecular docking showed that Naringenin-4'-O-glucoside, Poncirin, and Didymin target core proteins including AKT1 and EGFR to counteract oxidative damage. Transcriptomics, weighted gene co-expression network analysis (WGCNA), and molecular validation further demonstrated that transcription factors RcRAV, RcG2-like, and RcMYB drive antioxidant polyphenol accumulation by activating *RcPAL*, a key phenylpropanoid pathway gene. These findings establish the "transcription factor–*RcPAL*–polyphenol" cascade governing the high antioxidant activity of *Rubus chingii* green fruits, providing a theoretical basis for breeding high-medicinal-value varieties.

1. Introduction

Rubus chingii Hu, belonging to the genus Rubus in the *Rosaceae* family, is a perennial lianoid shrub with significant ecological and economic value [1]. This species is widely distributed naturally and cultivated on a large scale in eastern and south-central China, particularly in Jiangxi, Anhui, and Zhejiang provinces. Notably, due to its excellent quality and proven efficacy, *Rubus chingii* from Zhejiang has been officially listed among the "New Eight Zhejiang Herbs" (Xin Zhe Ba Wei) as an authentic medicinal material (Daodi herb), becoming a key characteristic economic berry and medicinal resource in the region. Throughout its developmental stages, the fruit exhibits distinctly different application values. The fully ripe red fruit, characterized by its bright color and sweet-sour taste, is commonly consumed fresh or processed as a nutritious food. Conversely, the unripe green fruit (known in traditional Chinese medicine as "Fupenzi") harbors immense medicinal potential [2-7]. The medicinal value of the green fruit is not only documented in various editions of the

Chinese Pharmacopoeia, but traditional Chinese medicine (TCM) also highly recognizes its clinical efficacy in "tonifying the kidneys, securing essence, reducing urination, nourishing the liver, and improving vision" [8]. In recent years, modern pharmacological and pharmacokinetic studies have further confirmed that extracts from the unripe green fruit exhibit significant biological activities in antioxidation, delaying cellular senescence, and regulating glucose and lipid metabolism homeostasis. For instance, in vivo experiments have explicitly reported that green fruit extracts can effectively intervene and reduce postprandial blood glucose levels in diabetic mice by ameliorating insulin resistance, demonstrating substantial potential in the prevention and adjuvant treatment of type 2 diabetes [9]. Furthermore, pectic polysaccharides specifically extracted from green fruits can significantly inhibit dietary fat absorption in the mouse intestine via competitive binding or steric hindrance effects, thereby exerting multiple physiological functions, including lipid reduction, gut microbiota improvement, and intestinal mucosal barrier protection [10].

The unripe green fruit of *Rubus chingii* is a highly complex repository of secondary metabolites, rich in various active molecules such as polyphenols, terpenoids, polysaccharides, and alkaloids. Among these, polyphenols are widely recognized as the core active components responsible for its broad pharmacological effects and are currently a focal point of research in phytochemistry and molecular pharmacognosy [2-7]. Plant polyphenols, a structurally diverse class of secondary metabolites primarily including flavonoids, flavonols, anthocyanins, and isoflavones, possess exceptional electron-donating and free-radical-quenching capabilities due to the abundance of phenolic hydroxyl groups in their molecular structures. Consequently, they exhibit remarkable biological functions in antioxidation, anti-tumor, anti-inflammation, and neuroprotection [11-13]. Extensive pathological studies indicate that oxidative damage is a pathological process triggered when the production rate of reactive oxygen species (ROS) or free radicals in the body exceeds the clearance capacity of the endogenous antioxidant defense system, leading to an imbalance in intracellular redox homeostasis. This excessive oxidative stress directly attacks biological macromolecules such as cell membrane lipids, proteins, and DNA, thereby inducing or accelerating the onset and progression of a series of chronic degenerative diseases, including various malignancies, cardiovascular diseases, and chronic inflammation-related syndromes [14-15]. Therefore, effectively regulating and reversing oxidative damage necessitates the intervention of exogenous antioxidants. Antioxidants are broadly defined as any substance that, when present at low concentrations, significantly delays, prevents, or eliminates the oxidation of a target molecule [16]. Maintaining a healthy antioxidant defense system in the human body depends not only on endogenous enzymes but also largely on the dietary intake of plant-based foods rich in natural antioxidants [16]. With the development of modern nutrition and preventive medicine, an increasing number of plant resources rich in natural polyphenols have been exploited. Their comprehensive antioxidant efficacy is often directly determined by the abundance and structural characteristics of their phenolic compounds. For example, specific flavonoids—kaempferol-3-O-rutinoside and quercetin-3-O-rutinoside—abundant in

black wolfberry (*Lycium ruthenicum*) significantly enhance the ROS-scavenging efficiency of cultured cells in vitro [17]. During a specific temperature-varying drying process, the increase in total phenolic and flavonoid contents in *Chrysanthemum morifolium* directly drives a leap in its overall antioxidant capacity [18]. Comparative studies on various teas have revealed a strict dose-dependent relationship between the core antioxidant capacity of tea infusions and their absolute polyphenol content [19]. Flavonoids isolated and purified from the traditional spice *Amomum tsao-ko* have been proven to be excellent free radical scavengers [20]. Furthermore, in vivo and in vitro experimental models of tangerine peel (Chenpi) have cross-validated the deep association between its flavonoid components and potent antioxidant abilities [21].

Notably, previous studies have astutely observed that during the ripening process of *Rubus chingii* fruits from green to red, their internal polyphenol profile undergoes drastic spatiotemporal dynamic reprogramming. This serves as the molecular basis for why green fruits possess higher medicinal value, whereas red fruits lean more toward edible attributes [5-6]. In recent years, with the rapid advancement of plant genomics and transcriptomics, researchers have successfully identified several key structural genes and transcription factors involved in regulating polyphenol biosynthesis in *Rubus chingii*. For instance, transcription factors such as RcWRKY and RcbZIP, along with key enzyme genes like RcUGT and Rc4CL, have been proven to exert crucial transcriptional activation or catalytic roles in this process [22-24]. However, existing molecular biology studies predominantly focus on the overall accumulation of polyphenols, without deeply dissecting and precisely anchoring which specific genes and transcription factors specifically drive the synthesis of polyphenols with "high antioxidant activity." Consequently, merely increasing the total polyphenol content through conventional means may not achieve a synchronous enhancement of its core medicinal value. With continuous progress in high-resolution metabolomics and bioinformatics, the strategy of deeply integrating metabolomics with network pharmacology has been successfully applied to mine key antioxidant metabolites in various plants. For example, 26 core metabolites targeting the antioxidant network were precisely identified in sour jujube [25]; 6 key molecules capable of specifically binding to antioxidant-related proteins such as CDK1, EGFR, and SRC were discovered in carrots [26]; 16 phenolic acid metabolites targeting the PI3K-AKT oxidative stress signaling pathway were found in strawberries [27]; and 29 key antioxidant metabolites that target and regulate core proteins like AKT1, EGFR, and MMP9 were identified in onions [28]. In contrast, for *Rubus chingii*, which specific polyphenol components truly contribute to its exceptional antioxidant activity, and what the precise transcriptional regulatory mechanisms of these core active substances are, remain unresolved mysteries. In light of this, the present study innovatively proposed and implemented a systematically integrated research strategy combining "metabolomics + network pharmacology + molecular docking." Building upon this, we deeply integrated transcriptomic analysis, aiming to preliminarily elucidate the molecular regulatory networks underlying the targeted accumulation of these antioxidant-related phenolic metabolites from a multidimensional "phenotype-metabolite-target-gene" perspective. Concurrently, to ensure the rigor of

the multi-omics prediction results, this study further functionally validated the mined key structural genes and their upstream transcriptional regulators through in vitro and in vivo experimental systems, including tobacco transient overexpression, the dual-luciferase (Dual-LUC) reporter assay, and yeast one-hybrid (Y1H) assays. The findings of this study not only systematically elucidate the material basis and genetic regulatory mechanisms of the high antioxidant activity in *Rubus chingii* green fruits but also provide a solid theoretical foundation and valuable genetic resources for the subsequent targeted breeding of superior medicinal *Rubus chingii* cultivars with high beneficial polyphenol contents via marker-assisted selection or genetic engineering.

2. Result

2.1 Comparison of physiological indicators and their correlations

To investigate the dynamic changes in physiologically active substances and their functions during fruit development, this study initially measured and compared the total phenolic content (TPC) across different developmental stages. The results revealed distinct variations in TPC during fruit maturation. A cross-stage comparison indicated that the TPC reached its peak at the green fruit stage, which was significantly higher than that at all other developmental stages according to statistical analysis (Fig. 1A). This phenomenon suggests that the biosynthesis and accumulation of phenolic compounds are highly active during the early stages of fruit development.

To evaluate the in vitro antioxidant activity, three classical assays—ABTS free radical scavenging, DPPH free radical scavenging, and ferric-reducing antioxidant power (FRAP)—were employed to comprehensively assess the antioxidant potential of the fruits at different stages. The results demonstrated that the variation trends of these three antioxidant indicators were highly consistent with the dynamic changes in TPC. Specifically, the green fruit stage exhibited the strongest antioxidant activity in the ABTS, DPPH, and FRAP assays, and its comprehensive antioxidant capacity was significantly superior to that of the other developmental stages (Fig. 1B, C, D). This indicates that green fruits possess exceptional physiological efficacy in scavenging free radicals and reducing metal ions.

To further elucidate the intrinsic relationship between antioxidant capacity and the content of bioactive compounds, a correlation analysis was conducted between the TPC and the three antioxidant indicators (ABTS, DPPH, and FRAP) across all stages. The analysis revealed a highly significant positive correlation between TPC and the ABTS, DPPH, and FRAP values (Fig. 1E). Notably, the correlation coefficients (r values) between TPC and these three antioxidant indicators were all greater than 0.9, indicating a remarkably tight association. This highly significant and strong positive correlation robustly demonstrates that total phenolic compounds serve as the core material basis for the potent antioxidant activity observed throughout fruit development, particularly at the green fruit stage.

2.2 Comparison of metabolomic profiles across different developmental stages of *Rubus chingii* Hu and mining of key antioxidant metabolites

To comprehensively elucidate the dynamic metabolic networks during the fruit development of *Rubus chingii* Hu, this study conducted an in-depth evaluation of its metabolomic profiles using liquid chromatography-mass spectrometry (LC-MS). First, principal component analysis (PCA) revealed that, based on the overall metabolite abundance profiles, fruit samples from the five developmental stages (green, yellow, orange, pink, and red) formed distinct and tight independent clusters on the two-dimensional score plot (Fig. 2A). This indicates significant spatial distribution differences and strong stage-specificity in the overall metabolite profiles across different ripening stages.

Regarding metabolite identification, a total of 1,064 polyphenolic metabolites were successfully annotated. Systematic classification revealed that at the Class I level, flavonoids were absolutely dominant, accounting for 48.9% of the total, whereas stilbenes exhibited the lowest diversity, comprising only 1.9% (Fig. 2B). Further refinement to the Class II level showed that phenolic acids were the most abundant (29.7%), while proanthocyanidins were the least represented (1.1%) (Fig. 2B). A cross-stage comparison indicated that 1,018, 1,010, 979, 1,007, and 967 polyphenolic metabolites were stably detected in the green, yellow, orange, pink, and red fruits, respectively (Fig. 2C). This suggests that, although the relative abundances of these metabolites may fluctuate during development, the overall diversity of polyphenolic species remains relatively stable across all stages with minimal variation.

To maximize the separation between groups and identify key variables, an orthogonal partial least squares-discriminant analysis (OPLS-DA) model was constructed. The predictive model highlighted highly significant metabolic differences between the green fruit and the fruits from the other four developmental stages (Fig. S1). Subsequent permutation testing confirmed the robustness of the model; the goodness-of-fit parameter (R^2Y) reached 1, and the predictability parameter (Q^2) exceeded 0.99, indicating an exceptionally high explanatory power without overfitting (Fig. S2). Quantitative profiling of the differentially expressed metabolites (DEMs) revealed that the lowest number of DEMs was observed between the green and yellow fruits (99), whereas the highest number was found between the green and fully mature red fruits (396) (Fig. 3A). Furthermore, compared to other stages, the green fruits exhibited a significantly higher number of up-regulated DEMs than down-regulated ones (Fig. 3A). An in-depth classification of these DEMs revealed that the vast majority belonged to flavonoids and phenolic acids (Fig. 3B), suggesting that these two classes of compounds are the core components driving the turnover of metabolic phenotypes during fruit development.

To further identify metabolic modules closely associated with antioxidant activity, Weighted Metabolite Co-expression Network Analysis (WMCNA) was employed. The module-trait relationship heatmap demonstrated that the turquoise module exhibited a highly significant positive correlation with TPC as well as the three antioxidant capacities (ABTS, DPPH, and FRAP) (Fig. 3C). A total of 493 polyphenolic metabolites were clustered into this turquoise module, with flavonoids

and phenolic acids remaining dominant, accounting for 40.7% and 33.9%, respectively (Fig. 3D). Further extraction and classification of the 313 DEMs within this module revealed that its primary constituents were still flavonoids (39.9%) and phenolic acids (34.2%) (Fig. 3E).

To precisely identify the core functional molecules responsible for antioxidant activity, a stringent correlation threshold (Pearson $r > 0.8$ and $P < 0.05$) was applied, resulting in the identification of 90 key metabolites that were significantly and positively correlated with TPC and all antioxidant indicators (Fig. 3F). Among these 90 key antioxidant metabolites, phenolic acids and flavonoids accounted for 40.0% and 33.3%, respectively (Fig. 3G). Ultimately, based on network topological properties, the intra-module connectivity (kWithin values) of these 90 key metabolites was calculated, successfully pinpointing the top five core hub metabolites. These included PDP152114 (Neosakuranetin), PDP152802 (8-Hydroxyapigenin 8-(6"-E-p-coumaroylglucoside)), Waln002419 (1'-O-Galactoyl p-Coumaric acid), PDP213721 (3-(P-Hydroxyphenyl)pyruvate), and Lmyp004318 (Kaempferol-3-O-(6"-p-Coumaroyl)galactoside). According to the Class II classification criteria, these five core metabolites belong to chalcones, flavones, phenolic acids, phenolic acids, and flavonols, respectively (Table S3). These findings provide critical molecular targets for elucidating the material basis and metabolic regulatory networks underlying the potent antioxidant activity of *Rubus chingii* Hu fruits.

2.3 Prediction of the medicinal value and underlying targeting mechanisms of key antioxidant metabolites

To further explore the pharmacological mechanisms by which the identified key antioxidant metabolites alleviate oxidative damage and potentially intervene in related diseases, this study employed an integrated approach combining network pharmacology and molecular docking. First, potential targets of these key antioxidant metabolites were comprehensively screened and mapped by jointly searching authoritative databases, including TCMSP, SwissTargetPrediction, and GeneCards. As a result, eight key antioxidant metabolites with significant medicinal potential were successfully identified, comprising two tannins, five flavonoids, and one phenolic acid. These eight core metabolites were mapped to a total of 270 target genes closely associated with oxidative damage. Consequently, a "metabolite-target" interaction network was constructed (Fig. 4A), highlighting the multi-target synergistic characteristics of these bioactive compounds.

To further elucidate the synergistic regulatory mechanisms among these targets, the identified targets were imported into the STRING database to construct a protein-protein interaction (PPI) network. Network topological analysis revealed highly dense interactions among 266 target proteins, encompassing a total of 3,204 tight interaction edges, which indicates exceptionally strong network connectivity. Based on the node degree values, the top 10 core hub targets were ranked and identified as AKT1, EGFR, STAT3, ESR1, HSP90AA1, HIF1A, BCL2, SRC, JUN,

and PTGS2 (Fig. 4B). These core targets play crucial roles in regulating cell proliferation, apoptosis, and oxidative stress response networks.

Subsequently, a KEGG pathway enrichment analysis was performed on the 270 oxidative damage-related targets. The results demonstrated that these targets were significantly enriched in pathways in cancer, the HIF-1 signaling pathway, the NF-kB signaling pathway, and chemical carcinogenesis-reactive oxygen species (Fig. 4C). This finding suggests that these antioxidant metabolites may exert their cytoprotective and disease-preventive effects by modulating inflammatory responses and signaling cascades associated with hypoxia and oxidative stress.

In parallel, Gene Ontology (GO) enrichment analysis systematically elucidated the biological functions of these targets across three dimensions (Fig. 4D). In the Molecular Functions (MF) category, the targets were primarily enriched in protein kinase activity, oxidoreductase activity, and protein tyrosine kinase activity. In the Biological Processes (BP) category, significant enrichment was observed in response to hormone, cell surface receptor protein tyrosine kinase signaling pathway, and regulation of inflammatory response. In the Cellular Components (CC) category, the targets were predominantly localized to the perinuclear region of cytoplasm, signaling receptor complex, and dendrite. Together, these enrichment results systematically delineate the subcellular localization of the targeted proteins and the specific physiological and biochemical processes in which they participate.

Finally, to validate the reliability of the network pharmacology predictions and explore intermolecular affinities, the top 10 core hub proteins from the PPI network were selected for molecular docking analysis with the eight key antioxidant metabolites. The binding energy assessments revealed that multiple receptor-ligand complexes exhibited remarkably strong binding affinities. Specifically, the binding energies of the target protein AKT1 with the metabolites HJN087 (Naringenin-4'-O-glucoside), mws0791 (Poncirin), and MWSslk252 (Didymin) were all lower than -10 kcal/mol. Similarly, the binding energy between the target protein EGFR and the metabolite MWSslk252 (Didymin) was also below -10 kcal/mol (Fig. 5A). Generally, a binding energy of less than -5.0 kcal/mol indicates good binding activity, whereas a value lower than -10 kcal/mol signifies an exceptionally strong and spontaneous binding capacity between the ligand and the receptor. Subsequently, PyMOL software was utilized for the three-dimensional visualization of these high-affinity receptor-ligand complexes. This visualization clearly illustrated the spatial conformations of the small-molecule metabolites and their specific binding sites within the active pockets of the target proteins (Fig. 5B), thereby providing solid structural biological evidence for the pharmacological activities of these key antioxidant metabolites at the molecular level.

2.4 Comparative transcriptomic profiling across developmental stages of *Rubus chingii* Hu and identification of polyphenol regulatory genes

To elucidate the molecular mechanisms underlying the dynamic changes in polyphenols during fruit development at the whole-transcriptome level, comprehensive RNA-seq analysis was performed on samples from five distinct developmental stages. The two-dimensional score plot from principal component analysis (PCA) clearly demonstrated that, based on the global gene expression profiles, samples from the five developmental stages exhibited highly independent and regular spatial clustering (Fig. 6A). This indicates that the fruits underwent significant global transcriptional reprogramming during the ripening process. Statistical analysis of the differentially expressed genes (DEGs) further revealed the magnitude of transcriptional changes between adjacent developmental stages: the transcriptomic difference was minimal between the green and yellow fruit stages, with only 2,775 DEGs identified, whereas the most drastic difference occurred between the green and fully mature red fruit stages, representing the broadest developmental span, which yielded 9,173 DEGs (Fig. 6B). To explore the biological functions of these DEGs, KEGG pathway enrichment analysis was conducted. The results showed that in all comparisons between the green fruit stage and subsequent ripening stages, the DEGs were consistently and highly enriched in the "phenylpropanoid biosynthesis" pathway (Fig. 6C). This strongly implies that the exceptional activity of this metabolic pathway during the green fruit stage is a crucial driver for the massive accumulation of polyphenols.

To precisely identify gene clusters closely associated with antioxidant capacity, weighted gene co-expression network analysis (WGCNA) was employed. This analysis successfully delineated a core "turquoise" module comprising 8,039 genes. The eigengene of this module exhibited highly significant positive correlations with total phenolic content (TPC) and the three antioxidant capacity indices (ABTS, DPPH, and FRAP) (Fig. 6D). By intersecting the genes within the turquoise module with those enriched in the phenylpropanoid pathway, we successfully identified the shared key rate-limiting enzyme genes responsible for catalyzing the biosynthesis of polyphenolic metabolites, including flavonoids, phenolic acids, lignans, coumarins, and condensed tannins. These genes belong to the *PAL* (*phenylalanine ammonia-lyase*) and *4CL* (*4-coumarate:CoA ligase*) families (Fig. 7A). A transcriptomic expression heatmap visually displayed the dynamic transcriptional patterns of these structural genes: the transcript abundance of *LG06.4119* (a member of the *RcPAL* gene family) exhibited a continuous decline as fruit ripening progressed, whereas the expression levels of *LG06.2544* and *LG06.2545* (members of the *Rc4CL* gene family) displayed a fluctuating pattern, characterized by an initial decrease followed by a slight upregulation during the late ripening stages (Fig. 7B).

To identify the upstream molecular switches regulating these key structural genes, we further screened for differentially expressed transcription factors (TFs) within the turquoise module. Based on network topology parameter analysis, five differentially expressed TFs (LG06.1741, LG01.3497, LG02.4694, LG05.66, and LG02.4611) were selected. Their intra-modular connectivity (kWithin values) ranked in the top five among all TFs in the turquoise module (Table S4), thereby establishing them as core

regulatory factors. Pearson correlation analysis between these five key TFs and the three aforementioned structural genes revealed that the TFs exhibited highly significant positive correlations exclusively with the expression of *LG06.4119* (*RcPAL*) (Fig. 7C). Crucially, promoter sequence prediction analysis confirmed that the promoter region of LG06.4119 contains specific cis-acting elements (binding sites) for the RAV, G2-like, and MYB transcription factor families (Fig. 7D), providing direct sequence-structural evidence for the targeted binding of these TFs to their target gene. Furthermore, integrated transcriptomic and metabolomic analysis revealed that the expression level of *LG06.4119* (*RcPAL*) was significantly and positively correlated with the abundance of 76 key antioxidant polyphenolic metabolites (Pearson $r > 0.8$, $P < 0.05$). Metabolic pathway analysis confirmed that these compounds are all located in the downstream branches of the RcPAL-catalyzed reaction (Table S5). Based on this multidimensional chain of evidence, we ultimately constructed a cascade regulatory network model in which the transcription factors LG01.3497 (RcRAV), LG05.66 (RcG2-like), and LG02.4611 (RcMYB) target and activate *RcPAL* expression, thereby driving the biosynthesis of key downstream polyphenolic metabolites and ultimately enhancing the polyphenol content in green fruits (Fig. 7E).

2.5 Experimental validation of key polyphenol regulatory genes identified from transcriptomic analysis

To verify the accuracy of the RNA-seq data and the reliability of the gene expression profiles, the relative expression levels of the identified core structural gene (*RcPAL*) and three key transcription factors (RcRAV, RcG2-like, and RcMYB) were first validated using quantitative real-time PCR (RT-qPCR). The results demonstrated that the relative expression levels of all four genes exhibited a continuous and significant downward trend throughout the fruit ripening process (Fig. 8A). These dynamic expression patterns were highly consistent with the RNA-seq results, thereby confirming the reliability of the transcriptomic data.

To determine the spatial distribution of these proteins where they exert their biological functions, subcellular localization assays were conducted. Fluorescence microscopy revealed that the RcPAL signal was widely distributed throughout the cytoplasm, consistent with its expected role as a metabolic enzyme catalyzing biochemical reactions in the cytosol. Conversely, the fluorescence signals of the three transcription factors (RcRAV, RcG2-like, and RcMYB) were specifically localized to the nucleus (Fig. 8B), aligning with the typical characteristics of transcription factors that bind to DNA and regulate gene transcription within the nucleus.

To validate the in vivo biological function of the *RcPAL* gene, an overexpression construct was generated and used for transient expression assays in tobacco. Phenotypic observations revealed that, compared with the wild-type (WT) control, tobacco leaves overexpressing *RcPAL* exhibited obvious yellowing (Fig. 8C), suggesting a potential overaccumulation of specific secondary metabolites, such as

flavonoids or polyphenols. Subsequent biochemical quantification further confirmed that the total phenolic content (TPC) in the leaves of the overexpressing plants was significantly higher than that in the WT plants (Fig. 8D). This provides direct evidence for the core positive regulatory role of *RcPAL* in promoting polyphenol biosynthesis.

To investigate the transcriptional activation effects of the three key transcription factors on the *RcPAL* promoter, dual-luciferase (Dual-LUC) reporter assays were conducted. Effector constructs containing the transcription factor coding sequences and a reporter construct harboring the target gene promoter fragment were generated (Fig. 8E). Qualitative in vivo bioluminescence imaging visually demonstrated that, compared with the empty vector control, co-infiltration with any of the three transcription factors induced substantially stronger luminescence signals (Fig. 8F). Subsequent quantitative analysis of luciferase activity confirmed that the LUC/REN ratios in samples co-transformed with these transcription factors were significantly higher than that of the control (Fig. 8G). This confirms that RcRAV, RcG2-like, and RcMYB possess significant transcriptional activation activity toward the *RcPAL* promoter.

Finally, to validate the in planta Dual-LUC results and confirm the direct physical interactions between these proteins and the DNA sequence, yeast one-hybrid (Y1H) assays were performed. The results clearly showed that only the yeast strains co-transformed with the transcription factors and the target promoter sequence could survive and grow normally on the selective dropout medium, whereas the negative control strains could not (Fig. 8H). These in vitro findings corroborate the in vivo Dual-LUC results, providing conclusive evidence that these three transcription factors can directly bind to the promoter region of *RcPAL* to exert specific transcriptional regulatory functions.

3 Discussion

3.1 Dynamic evolution of antioxidant capacity and evaluation of medicinal value across developmental stages of *Rubus chingii*

The development and utilization of traditional medicinal plants, the selection of the harvesting period directly determines the quality and clinical efficacy of the herbal material. A central question addressed in this study is why the Chinese Pharmacopoeia and traditional Chinese medicine principles advocate for the use of green, unripe fruits (known as Fupenzi) rather than mature fruits for medicinal purposes. Antioxidant capacity, a critical metric for evaluating the potential of medicinal plants to prevent and alleviate various chronic diseases induced by oxidative stress (e.g., cardiovascular diseases, neurodegenerative disorders, and metabolic syndrome), provides direct biophysical evidence to answer this question. Our in vitro antioxidant evaluations revealed that the green fruit stage exhibited the most robust antioxidant capacity, as demonstrated by both radical scavenging assays (ABTS and DPPH) and the metal ion reducing power assay (FRAP). Notably, this

capacity exhibited a significant and a marked decline as the fruit matured. From the perspective of the antioxidant defense system, this dynamic evolutionary pattern provides a solid scientific basis for the superior medicinal and health-promoting value of green fruits.

Further biochemical quantification and correlation analyses elucidated the material basis underlying this phenomenon. We found that the accumulation pattern of total phenolic content (TPC) highly coincided with the trajectory of antioxidant capacity, peaking at the green fruit stage and decreasing with maturity. Statistical analysis confirmed a highly significant positive correlation between TPC and the ABTS, DPPH, and FRAP values ($P < 0.01$). Polyphenolic compounds, characterized by abundant phenolic hydroxyl groups in their structures, can effectively quench free radicals by donating hydrogen atoms or electrons, making them the most crucial non-enzymatic antioxidants in plants. This finding is highly consistent with studies on various other medicinal and edible plants. For instance, during the fermentation of *Dendrobium officinale*, fluctuations in TPC were significantly and positively correlated with ABTS and DPPH radical scavenging rates [41]. Similarly, the TPC in different solvent extracts of Pellionia repens directly determined their performance in ABTS, DPPH, and FRAP assays [42]. Furthermore, comparative studies on 10 rosaceous flower teas [43] and 10 fruits [44] consistently identified the enrichment of polyphenols as the core driver for enhanced DPPH antioxidant activity. Synthesizing our experimental data with existing literature, it can be unequivocally concluded that the massive accumulation of polyphenolic secondary metabolites during early development endows the green fruits of *Rubus chingii* with superior antioxidant efficacy, thereby establishing the material foundation for its use as a high-quality traditional Chinese medicine.

3.2 Stage-specific profiling of the *Rubus chingii* fruit polyphenol metabolome and identification of core antioxidants

To determine at the molecular level which specific metabolites confer the potent antioxidant capacity of green fruits, this study utilized high-resolution liquid chromatography-mass spectrometry (LC-MS) to deeply profile the polyphenol metabolome across the entire fruit developmental cycle. A total of 1,064 polyphenolic metabolites were identified. Comparative analysis revealed that the compositional profile of polyphenolic metabolites remained highly similar and stable across different developmental stages. This observation strongly implies that the key driving force behind the differential antioxidant capacities across stages is not the qualitative presence or absence of specific metabolites, but rather the quantitative fluctuations in their abundance. In terms of chemical classification, flavonoids and phenolic acids overwhelmingly dominated the overall metabolic pool.

The analysis of differentially accumulated metabolites (DAMs) further corroborated this inference. The results demonstrated that, compared to other mature stages, the green fruit stage not only possessed the highest number of significantly upregulated polyphenolic DAMs, but these highly abundant compounds were also heavily

concentrated within the flavonoid and phenolic acid classes. Flavonoids and phenolic acids typically feature multiple conjugated double bonds and active hydroxyl groups; this specific chemical architecture endows them with exceptional electron delocalization and free radical-trapping capabilities. By correlating phenotypic data with weighted gene co-expression network analysis (WGCNA), we precisely anchored 90 core DAMs within the "turquoise" module, which exhibited a highly significant positive correlation with antioxidant indicators (TPC, ABTS, DPPH, FRAP). The composition of these core DAMs was again predominantly flavonoids and phenolic acids.

Based on network topological parameters (kWithin values), we further quantified the centrality of these metabolites within the co-expression network and successfully identified five critical hub metabolites: PDP152114 (Neosakuranetin), PDP152802 (8-Hydroxyapigenin 8-(6"-E-p-coumaroylglucoside)), Waln002419 (1'-O-Galactoyl p-Coumaric acid), PDP213721 (3-(P-Hydroxyphenyl)Pyruvate), and Lmyp004318 (Kaempferol-3-O-(6"-p-Coumaroyl)galactoside). Strikingly, all five metabolites with the highest network weights belong exclusively to the flavonoid or phenolic acid classes. Extensive previous pharmacological research has thoroughly documented that flavonoids and phenolic acids are vital natural active molecules for improving the human antioxidant defense system and intervening in oxidative damage-related diseases [45]. Our study not only reiterates the importance of these two classes of compounds at a systems level but also specifies the exact chemical targets responsible for the high antioxidant activity of *Rubus chingii* green fruits at the single-molecule resolution, providing a high-precision material basis for its targeted development in modern phytomedicine and functional foods.

3.3 Network pharmacology and molecular docking-based prediction of targeting mechanisms and medicinal potential of key metabolites

Having identified the core antioxidant compounds, exploring the disease networks and signaling pathways these key metabolites might modulate in the human body is a crucial step toward the modernization of traditional Chinese medicine. Through network pharmacology predictions, we found that a core cluster of just eight key metabolites could map to as many as 270 disease targets closely related to oxidative damage. This "multi-component, multi-target" paradigm not only theoretically substantiates the multidimensional antioxidant and cytoprotective functions of *Rubus chingii* green fruits but also aligns with the synergistic mechanisms characteristic of traditional Chinese medicine.

Topological analysis of the protein-protein interaction (PPI) network revealed highly complex interactions among these 266 targets, with AKT1 and EGFR emerging as the central hub genes. AKT1 and EGFR are not only classical receptors and kinases that regulate cell proliferation, differentiation, and tumor biology, but they have also been widely recognized in recent years as critical defense hubs for cellular responses to oxidative stress and the maintenance of redox homeostasis [25-28, 34]. Molecular

docking provided thermodynamic validation for these predictions. The results demonstrated that the binding energies between several key metabolites and both AKT1 and EGFR were lower than -10 kcal/mol (e.g., AKT1 with HJN087, mws0791, and MWSslk252; EGFR with MWSslk252). In molecular docking evaluation systems, such low binding energies indicate that the small molecule ligands can spontaneously, easily, and stably dock into the active pockets of the target proteins, forming robust physicochemical bonds. This finding resonates strongly with existing literature; for example, alkaloid metabolites from Fritillaria have been shown to directly bind and activate AKT1, thereby initiating downstream antioxidant cascades [34]. Similarly, the soy-derived isoflavone glycitin can targetedly activate EGFR and its downstream NRF2 master antioxidant signaling pathway in both cellular and zebrafish models, significantly upregulating the expression of endogenous antioxidant enzymes such as SOD, CAT, and GSH [46].

Furthermore, KEGG pathway and GO functional enrichment analyses consistently indicated that these 270 intersecting targets are significantly enriched in pathways related to cancer development and antioxidant stress. Given that AKT1 plays a central role in survival signaling across various malignancies, including breast, liver, and colorectal cancers [47-49], and that EGFR is an established first-line target for the targeted therapy of non-small cell lung cancer and hepatocellular carcinoma [50-51], our results strongly suggest that the core polyphenolic metabolites in *Rubus chingii* green fruits likely alleviate in vivo oxidative damage while simultaneously exerting potential anti-tumor or chemopreventive effects via high-affinity binding and regulation of AKT1 and EGFR. This points to promising new research directions for expanding the clinical indications of this botanical drug.

3.4 Transcriptome-driven identification and functional validation of key structural genes and their upstream transcriptional regulatory networks for polyphenol biosynthesis

The spatiotemporal variations in metabolite abundance are fundamentally driven by the programmed remodeling of underlying gene expression. To elucidate the molecular mechanisms regulating the biosynthesis of the aforementioned key antioxidant polyphenols, this study precisely anchored the core structural genes of the phenylpropanoid biosynthesis pathway—*RcPAL* (*phenylalanine ammonia-lyase*) and *Rc4CL* (*4-coumarate:CoA ligase*)—through differential expression gene (DEG) analysis, WGCNA, and KEGG pathway mapping. Extensive plant physiological studies have confirmed that *PAL* and *4CL*, serving as rate-limiting and branch-point enzymes in phenylpropanoid metabolism, are decisive genes driving the carbon flux toward the synthesis of polyphenolics (including flavonoids, phenolic acids, and lignans) [52-53]. In our study, the transcript abundance of *RcPAL* exhibited a highly significant positive correlation with the content of 76 key polyphenolic metabolites, providing a combined transcriptomic-metabolomic explanation for the exceptionally high TPC in green fruits.

Building upon the identification of structural genes, we traced the regulatory cascade upstream. Through promoter cis-element analysis and network weight (kWithin) calculations, we screened three key transcription factors with high regulatory potential: RcRAV, RcG2-like, and RcMYB. Literature searches indicate that the role of the MYB transcription factor family in regulating plant secondary metabolism is widely recognized (e.g., VvMYB14 regulating polyphenol synthesis in grapes [56]). However, reports on the RAV and G2-like families regulating polyphenol biosynthesis are relatively scarce, with only sporadic findings in citrus (CitRAV regulating flavonoids [54]) and tea plants (CsG2-like1/2 regulating flavonoids [55]). Based on these findings, we proposed and constructed a transcriptional regulatory network model wherein RcRAV, RcG2-like, and RcMYB synergistically target and regulate the expression of *RcPAL*, thereby driving the massive biosynthesis of polyphenols in green fruits.

To translate these bioinformatic predictions into definitive biological facts, this study conducted a series of molecular biological validation experiments. First, heterologous overexpression of the *RcPAL* gene in tobacco resulted in a distinct phenotype: significant leaf yellowing. In plant physiology, tissue yellowing is often a macroscopic phenotypic manifestation of the hyper-accumulation of specific flavonoids or phenolic acids (e.g., phenolic acid enrichment in yellow tea [57], flavonoid accumulation in kiwifruit and tomato [58-59]). Biochemical assays confirmed the underlying cause of this phenotype, demonstrating that *RcPAL* overexpression significantly increased the TPC in tobacco leaves. This gain-of-function experiment is highly consistent with functional studies of homologous genes in Salvia miltiorrhiza (SmPAL [60]), soybean (GmPAL2.4 [61]), and Rhus chinensis (RchPAL [62]), substantiating the positive catalytic role of *RcPAL* in polyphenol biosynthesis. Subsequently, dual-luciferase (Dual-LUC) reporter assays and yeast one-hybrid (Y1H) systems provided direct molecular interaction evidence, confirming that RcRAV, RcG2-like, and RcMYB can not only physically bind to the promoter region of *RcPAL* but also effectively activate its transcriptional expression. While the binding and regulation of PAL genes by PeMYBs have been reported in Pleurotus eryngii [63], the identification of RcRAV and RcG2-like as novel upstream transcriptional activators of a PAL gene is reported here for the first time. These validation results not only perfectly close the evidence loop of this study—from phenotype and metabolome to transcriptome and molecular interactions—but also contribute a highly innovative theoretical addition to the transcriptional regulatory networks governing plant phenylpropanoid metabolism.

4. Materials and Methods

4.1 Plant Materials and Sample Collection

The experimental materials of *Rubus chingii* Hu (cv. Fuzhou) were obtained from plants cultivated for four years at the Zhejiang Academy of Forestry. Fruits at five developmental stages (green, yellow, orange, pink, and red) were harvested on May 16th, 2026. The collected samples were immediately frozen in liquid nitrogen and

ground into fine powder to facilitate subsequent physiological, metabolomic, transcriptomic, and RT-qPCR analyses. Three biological replicates were established for each developmental stage.

4.2 Measurement of Physiological Indicators

4.2.1 Determination of Total Polyphenol Content (TPC)

The total polyphenol content (TPC) was determined using the Folin-Ciocalteu method. Briefly, 0.1 g of the ground sample powder was sequentially mixed with 0.5 mL of 60% ethanol, 50 µL of Folin-Ciocalteu reagent, 50 µL of 12% Na_2CO_3, and 90 µL of distilled water. After the reaction, the absorbance was measured at 760 nm using a SpectraMax ABS Plus microplate reader (Molecular Devices, San Jose, CA, USA). Gallic acid was used as the standard to generate a calibration curve for calculating the TPC of the samples [29].

4.2.2 Ferric-Reducing Antioxidant Power (FRAP)

Assay Approximately 0.1 g of the liquid nitrogen-ground sample was extracted with 0.5 mL of 80% ethanol. The mixture was vortexed thoroughly and centrifuged at 10,000 × g for 10 min at room temperature. The resulting supernatant was collected and kept on ice for further analysis. A 6 µL aliquot of the supernatant was mixed with 180 µL of FRAP working solution and 14 µL of double-distilled water. After thorough mixing and a 10-min reaction, the absorbance was measured at 593 nm using a SpectraMax ABS Plus microplate reader (Molecular Devices, San Jose, CA, USA). $FeSO_4$ was used as the standard to construct a calibration curve, and the results were expressed as Fe^{2+} equivalent concentrations [30].

4.2.3 2,2'-Azino-bis(3-ethylbenzothiazoline-6-sulfonic acid) (ABTS)

Free Radical Scavenging Assay Approximately 0.1 g of the ground sample powder was mixed with 0.5 mL of 80% ethanol, vortexed, and centrifuged at 10,000 × g for 10 min at 4 °C. The supernatant was collected and kept on ice. A 10 µL aliquot of the supernatant was gently mixed with 200 µL of ABTS working solution and incubated for 5 min at room temperature. The absorbance was then measured at 734 nm using a SpectraMax ABS Plus microplate reader (Molecular Devices, San Jose, CA, USA). Distilled water was used instead of the sample extract for the blank control, following the same procedure. The free radical scavenging rate was calculated using the following formula: Scavenging rate (%) = [(Abs of control − Abs of sample) / Abs of control] × 100%. Trolox was used as the standard to generate a calibration curve, and the results were expressed as Trolox equivalent antioxidant capacity [31].

4.2.4 2,2-Diphenyl-1-picrylhydrazyl (DPPH) Free Radical Scavenging

Assay Approximately 0.1 g of the ground sample was mixed with 0.5 mL of 80% methanol, vortexed, and incubated in a water bath at 60 °C for 30 min. After centrifugation at 10,000 × g for 10 min at room temperature, the supernatant was

collected. A 10 μL aliquot of the supernatant was mixed with 190 μL of 0.1 mmol/L DPPH in absolute ethanol. The mixture was shaken and incubated in the dark for 30 min at room temperature. The absorbance was measured at 515 nm using a SpectraMax ABS Plus microplate reader (Molecular Devices, San Jose, CA, USA). For the control group, the DPPH solution was replaced with absolute ethanol, and for the blank group, the sample supernatant was replaced with 80% methanol. The free radical scavenging rate was calculated as follows: Scavenging rate (%) = [[Abs of blank − (Abs of sample − Abs of control)] / Abs of blank] × 100% [30].

4.3 Metabolomic analysis

Metabolomic profiling was performed using a widely targeted metabolomics approach provided by Metware Bio Inc. (Wuhan, China), based on an ultra-high-performance liquid chromatography-tandem mass spectrometry (UPLC-MS/MS) platform. The UPLC system utilized was an ExionLC™ AD series (Sciex, Singapore). For mass spectrometric detection, both low- and high-resolution platforms were employed: a QTRAP® 6500 system (Sciex, Singapore) and a TripleTOF® 6600 system (Sciex, Singapore), respectively.

Metabolites were extracted using a methanol-water extraction method. Briefly, 30 mg of powdered sample was accurately weighed into a 1.5 mL microcentrifuge tube. Subsequently, 1.5 mL of a -20°C pre-chilled 70% aqueous methanol solution containing internal standards was added, and the mixture was vortexed thoroughly. After centrifugation at 12,000 rpm for 3 min at 4°C, the supernatant was collected, passed through a 0.22 μm microporous membrane filter, and transferred to an autosampler vial for UPLC-MS/MS analysis.

Chromatographic separation was performed on an Agilent SB-C18 column (1.8 μm, 2.1 × 100 mm) maintained at 40°C. The mobile phase consisted of 0.1% formic acid in water (phase A) and 0.1% formic acid in acetonitrile (phase B). A gradient elution program was applied at a flow rate of 0.35 mL/min as follows: 5% B at 0 min, linearly increased to 95% B over 9.0 min, held at 95% B for 1.0 min, decreased to 5% B within 1.1 min, and finally re-equilibrated at 5% B for 2.9 min, resulting in a total run time of 14.0 min per injection. The injection volume was 2 μL.

Mass spectrometric detection was carried out using an electrospray ionization (ESI) source operated in both positive and negative ion modes. The ion source temperature was set to 500°C, with the ion spray voltage (IS) set at +5500 V in the positive mode and -4500 V in the negative mode. The curtain gas, ion source gas I (nebulizer gas), and ion source gas II (heater gas) were set to 25, 50, and 60 psi, respectively. The triple quadrupole mass spectrometer was operated in multiple reaction monitoring (MRM) mode. For each target metabolite, the declustering potential (DP) and collision energy (CE) were optimized for its specific precursor-to-product ion transition. Detection was performed by monitoring defined sets of MRM transitions in scheduled time windows corresponding to the retention time of each metabolite.

Metabolite identification was conducted by matching the mass-to-charge ratios (m/z), retention times, and MS/MS fragmentation spectra with an in-house authentic standards database (MWDB, MetWare Database). During data processing, isotopic signals, adduct ions (including $[M+K]^+$, $[M+Na]^+$, and $[M+NH_4]^+$), and fragment ions that were also present as higher molecular weight precursor ions were excluded to prevent redundancy.

A pooled quality control (QC) sample, generated by combining equal aliquots of all experimental samples, was analyzed throughout the analytical sequence. The relative quantification of metabolites was performed based on peak areas, which were normalized against the QC sample data to account for signal drift during the UPLC-MS/MS run.

Multivariate statistical analysis of the metabolomic data was performed on the MetWare Cloud platform (https://cloud.metware.cn/). First, Principal Component Analysis (PCA), an unsupervised pattern recognition method, was applied to obtain a preliminary overview of the overall metabolic differences between sample groups and the variability within each group. The PCA score plot visually illustrated the clustering and separation trends of the samples, indicating the presence of distinct metabolic profiles among the groups.

To further elucidate specific differences between comparison groups, a supervised Orthogonal Partial Least Squares Discriminant Analysis (OPLS-DA) was conducted. This model effectively maximizes the covariance related to group separation. The robustness and validity of the OPLS-DA model were rigorously evaluated through permutation testing (typically n = 200) to prevent overfitting. Based on the validated OPLS-DA model, Variable Importance in Projection (VIP) scores were calculated to assess the contribution of each metabolite to the inter-group discrimination.

The identification of differentially accumulated metabolites (DAMs) was based on a combination of multivariate and univariate statistical criteria. The screening thresholds were set as follows: a VIP score ≥ 1.0 from the OPLS-DA model and an absolute fold change (FC) ≥ 2.0 [32]. Metabolites satisfying all these criteria were considered statistically significant DAMs.

To identify co-expressed metabolite modules associated with antioxidant physiological traits, Weighted Metabolite Co-expression Network Analysis (WMCNA) was performed on all identified metabolites [33]. A signed, scale-free co-expression network was constructed using a soft-thresholding power determined by analyzing the network topology. Metabolites with highly similar abundance profiles across all samples were clustered into modules, with each module assigned a unique color label. A soft-thresholding power (β) of 17 was selected to achieve a scale-free topology fit index (R^2) of 0.85. During the dynamic tree-cutting process, the minimum module size was set to 20, and the merge cut height was set to 0.25. Subsequently, to pinpoint modules biologically relevant to antioxidant functions,

module eigengenes (MEs, the first principal component representing the overall abundance pattern of each module) were calculated. Correlations between the MEs and the measured antioxidant physiological indicators were then analyzed. Modules exhibiting a significant positive correlation ($p < 0.01$) with multiple antioxidant indicators were selected for further functional analysis. Finally, the relative importance of individual metabolites within the network was determined based on their intra-modular connectivity (kWithin) values.

4.4 Network pharmacology analysis

The SMILES IDs of the metabolites were retrieved based on their chemical names using the PubChem database (https://pubchem.ncbi.nlm.nih.gov/). The medicinal potential of these metabolites was evaluated using the Traditional Chinese Medicine Systems Pharmacology (TCMSP) database (https://www.tcmsp-e.com/). Metabolites were screened based on the criteria of oral bioavailability (OB) ≥30% and drug-likeness (DL) ≥ 0.18. The screened metabolites were then submitted to the SwissTargetPrediction database (https://swisstargetprediction.ch/) to predict their putative targets. Targets with a probability > 0.1 were considered potential metabolite targets [34]. Subsequently, targets related to oxidative damage were predicted using the GeneCards database (https://www.genecards.org/) [34]. The intersection of the predicted metabolite targets and the oxidative damage-related targets was identified to determine the common therapeutic targets [34].

The identified common targets were uploaded to the STRING database (https://cn.string-db.org/) to construct a protein-protein interaction (PPI) network. The resulting network was imported into Cytoscape (v3.10.0) to analyze the degree values of the targets. Finally, these key targets were submitted to the Metascape platform (https://metascape.org/) for Gene Ontology (GO) and Kyoto Encyclopedia of Genes and Genomes (KEGG) functional enrichment analyses.

4.5 Molecular docking Targets with high degree values in the PPI network were selected for molecular docking.

The 3D structures of the key target proteins were retrieved from the UniProt database (https://www.uniprot.org/), while the 3D structures of the corresponding key metabolites were obtained from the PubChem database (https://pubchem.ncbi.nlm.nih.gov/). Molecular docking was performed using AutoDockTools (v1.5.7) to predict the binding affinities between the metabolites and their targets. The interaction sites and docking conformations were visualized using PyMOL (v2.5.4).

4.6 Transcriptomic analysis

RNA sequencing (RNA-seq) was conducted by Metware Bio Inc. (Wuhan, China) using the DNBSEQ-T7+ sequencing platform (MGI Tech, Shenzhen, China). Clean reads were mapped to the *Rubus chingii* Hu reference genome using HISAT2 (v2.0.5)

[35]. Gene expression levels were quantified using the FeatureCounts tool (http://subread.sourceforge.net/), and fragments per kilobase of transcript per million mapped reads (FPKM) values were calculated based on transcript lengths. Differential expression analysis was performed based on the raw read counts using DESeq2 (v1.4.5). Genes with a fold change (FC) ≥ 2.0 and a false discovery rate (FDR) < 0.05 were defined as differentially expressed genes (DEGs) [36]. KEGG pathway enrichment analysis was subsequently performed on the DEGs identified among the different developmental stages.

To identify co-expressed gene modules associated with key antioxidant metabolites, weighted gene co-expression network analysis (WGCNA) was performed on all identified genes [37]. A signed scale-free co-expression network was constructed using an appropriate soft-thresholding power determined by network topology analysis. Based on highly similar expression patterns across all samples, genes were clustered into distinct modules, with each module assigned a unique color label. A soft-thresholding power (β) of 17 was selected to achieve a scale-free topology fit index (R^2) of 0.85. During the dynamic tree-cutting process, the minimum module size was set to 20, and the merge cut height was set to 0.25. Subsequently, to pinpoint biological modules related to antioxidant metabolites, module eigengenes (MEs, representing the first principal component of the overall expression pattern for each module) were calculated. Correlations between the MEs and the antioxidant physiological indicators were analyzed. Modules exhibiting a significant positive correlation ($p < 0.01$) with multiple antioxidant indicators were selected for further functional analysis. Transcription factors (TFs) within these key modules were predicted using the PlantTFDB database (https://planttfdb.gao-lab.org/prediction.php), and their relative importance within the network was evaluated based on their intra-modular connectivity (kWithin) values.

4.7 RT-qPCR assay

Total RNA was extracted using an RNA extraction kit (SEON, Zhangjiakou, China) and subsequently reverse-transcribed into cDNA using a reverse transcription kit (SEON, Zhangjiakou, China). Specific primers for quantitative real-time PCR (RT-qPCR) were designed using the "Batch q-PCR Primer Design" module in TBtools [38], and the synthesized primer sequences are listed in Table S1. The RT-qPCR assays were performed using the TB Green Premix Ex Taq (Takara, Dalian, China). RcActin was used as the internal reference gene, and the relative expression levels of the target genes were calculated using the 2^-ΔΔCt method [39].

4.8 Subcellular localization analysis

First-strand cDNA was synthesized using the PrimeScript™ RT reagent Kit with gDNA Eraser (Takara, Beijing, China). Gene-specific cloning primers were designed using Primer Premier 6 software [49] (primer sequences are detailed in Table S2). The open reading frames (ORFs) of *RcPAL*, *RcRAV*, *RcG2-like*, and *RcMYB* were

amplified using TaKaRa LA Taq® with GC Buffer (Takara, Beijing, China). Utilizing seamless cloning technology, the amplified ORFs (without stop codons) were inserted into the pAN580 vector, fused in-frame with a green fluorescent protein (GFP) tag at the N-terminus. The recombinant plasmids were then introduced into *Arabidopsis* mesophyll protoplasts via polyethylene glycol (PEG)-mediated transformation. Subcellular localization of the RcPAL, RcRAV, RcG2-like, and RcMYB fusion proteins was determined by observing the GFP fluorescence signals under a confocal laser scanning microscope with an excitation wavelength of 470 nm [40].

4.9 Overexpression of *RcPAL* in tobacco

The full-length ORF of *RcPAL* was inserted into the pBWA(V)HS vector driven by the CaMV 35S promoter using seamless cloning. The recombinant plasmid was transformed into *Agrobacterium tumefaciens* strain GV3101, which was subsequently used to infect *Nicotiana tabacum* (tobacco) leaves to generate transgenic plants [51]. After 60 days of growth, tobacco leaves were harvested, immediately frozen in liquid nitrogen, and ground into a fine powder. For total phenolic content (TPC) extraction, 0.1 g of the powdered sample was mixed sequentially with 0.5 mL of 60% ethanol, 50 μL of Folin-Ciocalteu reagent, 50 μL of 12% Na_2CO_3, and 90 μL of distilled water. After incubation, the absorbance of the mixture was measured at 760 nm using a SpectraMax ABS Plus microplate reader (Molecular Devices, San Jose, CA, USA). The TPC of the samples was calculated based on a standard curve generated using gallic acid as the standard [29].

4.10 Dual-luciferase and yeast one-hybrid assays

For the dual-luciferase (LUC) assay, the ORFs of RcRAV, RcG2-like, and RcMYB were cloned into the pGreenII 62-SK vector to serve as effectors. Concurrently, a 2,000 bp promoter fragment upstream of the *RcPAL* start codon (ATG) was inserted into the pGreenII 0800-LUC vector, upstream of the LUC reporter gene, to serve as the reporter. Both recombinant constructs were transformed into *Agrobacterium tumefaciens* strain GV3101 and co-infiltrated into tobacco leaves. The infiltrated tobacco plants were kept in the dark for 24 h and then transferred to a growth chamber at 25°C with a 16 h light / 8 h dark photoperiod for 2 days. The LUC bioluminescence signals were captured using a chemiluminescence imaging system (Tanon 5200). The activities of firefly luciferase (LUC) and Renilla luciferase (REN) were quantified using a Dual-Luciferase Reporter Assay Kit (Vazyme, DL101-01), and the relative LUC/REN ratio was calculated.

For the yeast one-hybrid (Y1H) assay, the ORFs of RcRAV, RcG2-like, and RcMYB were cloned into the pGADT7 vector to create the prey constructs. The 2,000 bp promoter region of *RcPAL* was amplified using the primers listed in Table S2 and inserted into the pAbAi vector to generate the bait construct. Autoactivation tests revealed that 100 ng/mL of Aureobasidin A (AbA) effectively inhibited the basal growth of the yeast. Subsequently, both the prey and bait constructs were

co-transformed into the Y1HGold yeast strain. Protein-DNA interactions were evaluated by observing yeast growth on SD/-Leu/-Ura dropout medium supplemented with 100 ng/mL AbA.

4.11 Data Analysis and Visualization

Pearson correlation analyses—including correlations among physiological indicators, between metabolites and physiological indicators, and between key metabolites and genes—were performed using the MetWare Cloud platform (https://cloud.metware.cn/). Bar charts were generated and statistical significance was annotated using GraphPad Prism 10. For multiple comparisons following a one-way analysis of variance (ANOVA), Tukey's honestly significant difference (HSD) test was applied.

5. Data Availability

All other data supporting the findings of this study are available from the corresponding author upon reasonable request. Requests for access should be directed to the lead contact, who will respond within two weeks. To maintain participant privacy and comply with ethical guidelines, certain sensitive datasets may require a formal data use agreement before release. Researchers interested in reproducing the analytical workflows can find the custom scripts and code used for statistical analysis and visualization in the Supplementary Materials section of this article.

6. Acknowledgements

The author(s) declared that financial support was received for this work and/or its publication. The authors (s) declare that they received financial support for the research and/or publication of thisarticle. This study was supported by Zhejiang Provincial ResearchInstitute Special Project (2026F1065-2-8).

7. Conflict of Interest

All financial, commercial or other relationships that might be perceived by the academic community as representing a potential conflict of interest must be disclosed. If no such relationship exists, authors will be asked to confirm the following statement:

The authors declare that the research was conducted in the absence of any commercial or financial relationships that could be construed as a potential conflict of interest.

8. Author Contributions

Conceptualization, X.X.; methodology, X.X.; software, X.X.; validation, X.X.; data curation, X.X.; writing−original draft preparation, X.X& S.C.; writing−review and editing, X.X.& S.C.; All authors have read and agreed to the published version of the manuscript.

9. References

[1] Chen M, Jia X, Hou D, et al. Fabrication of *Rubus chingii* Hu ellagitannins-loaded W/O and O/W emulsion gels: Structure, stability, in vitro digestion and in vivo metabolism[J]. International Journal of Biological Macromolecules, 2025, 295:

139656.

[2] Wu L, Jin Y, Chen H, et al. *Rubus chingii* Hu: ethnopharmacology, phytochemistry, quality control, functions and products[J]. Future Foods, 2024, 10: 100447.

[3] Shan C, Zhu Y, Bi H, et al. Preparation, structural characterization and health benefits of polysaccharides from *Rubus chingii* Hu: a review[J]. Frontiers in Pharmacology, 2025, 16: 1592046.

[4] Jia-Yun S, Si-Qi W, Kao-Hua L I U, et al. *Rubus chingii* Hu: An overview of botany, traditional uses, phytochemistry, and pharmacology[J]. Chinese journal of natural medicines, 2020, 18(6): 401-416.

[5] Li X, Jiang J, Chen Z, et al. Transcriptomic, proteomic and metabolomic analysis of flavonoid biosynthesis during fruit maturation in *Rubus chingii* Hu[J]. Frontiers in Plant Science, 2021, 12: 706667.

[6] Hua Y, Dai B, Luo Y, et al. Integrated analysis of multiple metabolome and transcriptome revealed the accumulation of flavonoids and associated molecular regulation mechanisms in *Rubus chingii* Hu at different developmental stages[J]. Plant Physiology and Biochemistry, 2023, 204: 108085.

[7] Chen Z, Jiang J, Shu L, et al. Combined transcriptomic and metabolic analyses reveal potential mechanism for fruit development and quality control of Chinese raspberry (*Rubus chingii* Hu)[J]. Plant Cell Reports, 2021, 40(10): 1923-1946.

[8] Xu Z, Zhang G, Chen J, et al. Role of *Rubus chingii* BBX gene family in anthocyanin accumulation during fruit ripening[J]. Frontiers in Plant Science, 2024, 15: 1427359.

[9] Jun Tan, Danshu Wang, Yu Lu, et al. Metabolic enzyme inhibitory abilities, in vivo hypoglycemic ability of palmleaf raspberry fruits extracts and identification of hypoglycemic compounds[J]. Food Science and Human Wellness, 2023, 12(4): 1232-1240.

[10] Xingxing Wang, Yupeng Liu, Yongbin Xu, et al. Structural characterization of a pectic polysaccharide from *Rubus chingii* Hu. unripe fruits and its efficacy in inhibiting intestinal lipid absorption in vivo[J]. Carbohydrate Polymers, 2025, 363: 123728.

[11] Kopustinskiene D M, Jakstas V, Savickas A, et al. Flavonoids as anticancer agents[J]. Nutrients, 2020, 12(2): 457.

[12] Brodowska K M. Natural flavonoids: classification, potential role, and application of flavonoid analogues[J]. European journal of biological research, 2017, 7(2): 108.

[13] Rha C S, Jeong H W, Park S, et al. Antioxidative, anti-inflammatory, and anticancer effects of purified flavonol glycosides and aglycones in green tea[J]. Antioxidants, 2019, 8(8): 278.

[14] Hu B, Ouyang Y, Zhao T, et al. Antioxidant hydrogels: antioxidant mechanisms, design strategies, and applications in the treatment of oxidative stress-related diseases[J]. Advanced healthcare materials, 2024, 13(11): 2303817.

[15] Forman H J, Zhang H. Targeting oxidative stress in disease: promise and limitations of antioxidant therapy[J]. Nature reviews Drug discovery, 2021, 20(9): 689-709.

[16] Halliwell B. Understanding mechanisms of antioxidant action in health and disease[J]. Nature Reviews Molecular Cell Biology, 2024, 25(1): 13-33.

[17] Du Y, Ma H, Liu Y, et al. Major quality regulation network of flavonoid synthesis governing the bioactivity of black wolfberry[J]. New Phytologist, 2024, 242(2): 558-575.

[18] Sun Y, Gao C, Wang C, et al. Metabolomics analysis reveals dynamic changes in the quality components and antioxidant activity capacity during variable temperature drying of Jinsihuangju (Chrysanthemum morifolium) tea[J]. Food Research International, 2026: 118915.

[19] Li L, Wen M, Hu W, et al. Non-volatile metabolite and in vitro bioactivity differences in green, white, and black teas[J]. Food Chemistry, 2025, 477: 143580.

[20] Huang Z, Zhao Y, Yang W, et al. Preparation of flavonoids from Amomum tsaoko and evaluation of their antioxidant and α-glucosidase inhibitory activities[J]. Food Chemistry: X, 2025, 25: 102177.

[21] Wang W, Zhang J, Liu C, et al. Metabolomics combined with extraction optimization and biochemical assays revealed flavonoids and in vitro and in vivo antioxidant activity of Ponkan Chenpi[J]. Food Research International, 2026: 118324.

[22] Xu X R, Cheng Y, Cheng S. Identification of the *RcWRKY* family in *Rubus chingii* and analysis of its regulatory mechanisms for flavonoid synthesis[J]. Frontiers in Plant Science, 2025, 16: 1728584.

[23] Xu X R, Lai J X, Cheng S. Identification of the *RcbZIP* gene family in *Rubus chingii* and analysis of the regulation of flavonoid synthesis by RcbZIP1 and RcbZIP12[J]. Frontiers in Plant Science, 2026, 17: 1769751.

[24] Shi Y, Shen M, Wei L, et al. The bZIP24-bZIP53 transcription factor complex regulates kaempferol 3-O-rutinoside biosynthesis in *Rubus chingii* by targeting 1, 6-rhamnosyltransferase[J]. Plant Physiology and Biochemistry, 2026, 232: 111131.

[25] Chen Y, Zeng X, Qin W, et al. Integrated Metabolomics and Network Pharmacology Reveal the Active Components and Potential Health-Beneficial Mechanisms of Different Jujube (*Ziziphus jujuba*) Cultivars[J]. Foods, 2026, 15(8): 1347.

[26] He C, Mkunga J J, Zhang D, et al. Metabolite-based color codes and antioxidant mechanisms in carrots: insights from untargeted metabolomics and bioinformatics[J]. Food Chemistry, 2025: 146637.

[27] Zeng Z, Xu L, Xu J, et al. In-depth profiling of Phenolics in strawberries and their potential modulatory effects on the oxidative stress-disease Axis: Insights from UHPLC-QTOF-MS-based untargeted metabolomics, network pharmacology, and molecular docking[J]. Food Chemistry, 2025, 489: 145044.

[28] He C, Mkunga J J, Zhang D, et al. Characterization of antioxidant qualities and exploration of mechanisms in different colored onions: Insights from metabolomics and systems biology[J]. Food Chemistry: X, 2026: 103955.

[29] Fan S, Cai T, Cao F, et al. Integrated metabolome and transcriptome profiling unveil the mechanisms of tissue-specific polyphenol synthesis in Chinese chestnut (*Castanea mollissima* BL.)[J]. Scientia Horticulturae, 2025, 353: 114498.

[30] Tao M, Zhang P, Wang T, et al. Identification of key quality indicators for Zigui navel orange varieties through multivariate analyses[J]. Food Chemistry: X, 2026: 103702.

[31] Guo L, Qiao J, Zhang L, et al. Metabolome reveals high nitrogen supply decreases the antioxidant capacity of blue honeysuckle (Lonicera caerulea L.) by regulating flavonoids[J]. Food Chemistry, 2025, 480: 143954.

[32] Sun P, Ge G, Sun L, et al. Metabolomics combined with physiology and transcriptomics reveal the regulation of key nitrogen metabolic pathways in alfalfa by foliar spraying with nano-selenium[J]. Journal of Nanobiotechnology, 2025, 23(1): 7.

[33] Zhou L, She J, Li Q, et al. Integrated multi-omics and network pharmacology reveals antioxidant-active metabolites and health benefits of Camellia oleifera seed oil[J]. Food Chemistry, 2025: 146913.

[34] Guo X, Chen X, Zeng M, et al. Revealing key antioxidant compounds and mechanisms in Fritillaria Bulbus by metabolomics and network pharmacology[J]. npj Science of Food, 2025, 9(1): 124.

[35] Wang L, Lei T, Han G, et al. The chromosome-scale reference genome of *Rubus chingii* Hu provides insight into the biosynthetic pathway of hydrolyzable tannins[J]. The Plant Journal, 2021, 107(5): 1466-1477.

[36] Bai Y, Zhu M, Du B, et al. Multi-omics analyses unveil the molecular mechanism

involving flavonoid-mediated color changes of different mango varieties[J]. Food Chemistry, 2025: 147663.

[37] Wang R, Shu P, Zhang C, et al. Integrative analyses of metabolome and genome-wide transcriptome reveal the regulatory network governing flavor formation in kiwifruit (*Actinidia chinensis*)[J]. New phytologist, 2022, 233(1): 373-389.

[38] Chen C, Wu Y, Li J, et al. TBtools-II: A "one for all, all for one" bioinformatics platform for biological big-data mining[J]. Molecular plant, 2023, 16(11): 1733-1742.

[39] Livak K J, Schmittgen T D. Analysis of relative gene expression data using real-time quantitative PCR and the $2^{-\Delta\Delta CT}$ method[J]. methods, 2001, 25(4): 402-408.

[40] Yoo SD, Cho YH, Sheen J. Arabidopsis mesophyll protoplasts: a versatile cell system for transient gene expression analysis. Nat Protoc. 2007;2(7):1565-1572. doi:10.1038/nprot.2007.199.

[41] Wu J, He T, Wang Z, et al. The dynamic analysis of non-targeted metabolomics and antioxidant activity of Dendrobium officinale Kimura et Migo by the synergistic fermentation of bacteria and enzymes[J]. LWT, 2024, 203: 116354.

[42] Lim W L, Wong F C, Abd Manan F, et al. Sequential ultrasound-hot water extraction of Tradescantia zebrina leaves: optimized bioactivities with limited gastrointestinal stability[J]. Food Innovation and Advances, 2025, 5(1): 37-44.

[43] Xiao Y, Qian W, Fan S, et al. Comparative study on the differences of non-volatile and volatile compounds in ten edible flower teas: An integrated multi-omics, molecular-docking and machine-learning approach[J]. LWT, 2026: 119121.

[44] Sun Y, Zhou M, Luo L, et al. Metabolic profiles, bioactive compounds and antioxidant activity of rosehips from Xinjiang, China[J]. LWT, 2023, 174: 114451.

[45] Lang Y, Gao N, Zang Z, et al. Classification and antioxidant assays of polyphenols: A review[J]. Journal of Future Foods, 2024, 4(3): 193-204.

[46] Liu X, Meng X, Liu D, et al. A rapid analysis method to discover antioxidant active components and mechanisms in soybean: untargeted metabolomics combined with network pharmacology and spectrum-effect relationship-component knockout-identification techniques[J]. Food Science and Human Wellness, 2025, 14(9): 9250620.

[47] Hinz N, Jücker M. Distinct functions of AKT isoforms in breast cancer: a comprehensive review[J]. Cell Communication and Signaling, 2019, 17(1): 154.

[48] Cai D, Zhong G C, Dai X, et al. Targeting FDFT1 reduces cholesterol and bile acid production and delays hepatocellular carcinoma progression through the

HNF4A/ALDOB/AKT1 axis[J]. Advanced science, 2025, 12(12): 2411719.

[49] Baba Y, Nosho K, Shima K, et al. Phosphorylated AKT expression is associated with PIK3CA mutation, low stage, and favorable outcome in 717 colorectal cancers[J]. Cancer, 2011, 117(7): 1399-1408.

[50] Paez J G, Janne P A, Lee J C, et al. EGFR mutations in lung cancer: correlation with clinical response to gefitinib therapy[J]. Science, 2004, 304(5676): 1497-1500.

[51] Jin H, Shi Y, Lv Y, et al. EGFR activation limits the response of liver cancer to lenvatinib[J]. Nature, 2021, 595(7869): 730-734.

[52] Liu S, Meng Z, Zhang H, et al. Identification and characterization of thirteen gene families involved in flavonoid biosynthesis in Ginkgo biloba [J]. Industrial Crops and Products, 2022, 188: 115576.

[53] Du L, Lu C, Wang Z, et al. GFAnno: integrated method for plant flavonoid biosynthesis pathway gene annotation [J]. Beverage Plant Research, 2024, 4(1).

[54] Zhao C, Liu X, Gong Q, et al. Three AP2/ERF family members modulate flavonoid synthesis by regulating type IV chalcone isomerase in citrus[J]. Plant Biotechnology Journal, 2021, 19(4): 671-688.

[55] Liu X, Cheng X, Cao J, et al. GOLDEN 2-LIKE transcription factors regulate chlorophyll biosynthesis and flavonoid accumulation in response to UV-B in tea plants[J]. Horticultural Plant Journal, 2023, 9(5): 1055-1066.

[56] Wu M, Huang D, Zhu S. GYSVd1 mediates phenolic synthesis in grape berries via the *VvMYB14-Vv4CL* pathway[J]. Postharvest Biology and Technology, 2026, 237: 114283.

[57] Jiang, C., J.-P. Ke, Z. Wang, et al. 2026. “ Phenolic Acids and Their Derivatives in Tea: Chemical Diversity, Processing Changes, Sensory Contributions, and Health Implications—A Comprehensive Review.” Comprehensive Reviews in Food Science and Food Safety 25, no. 4: e70553. https://doi.org/10.1111/1541-4337.70553

[58] Lan T, Bao S, Li X, et al. Pigment and transcriptome profiling of flesh yellowing during post-ripening of ‘Puyu’kiwifruit[J]. Postharvest Biology and Technology, 2026, 234: 114109.

[59] Li Y, Meng F, You H, et al. SlWRKY14 integrates carotenoid and flavonoid biosynthetic pathways to regulate coloration and quality of tomato fruits[J]. Cell Reports, 2025, 44(10).

[60] Yu H, Li D, Yang D, et al. SmKFB5 protein regulates phenolic acid biosynthesis by controlling the degradation of phenylalanine ammonia-lyase in *Salvia miltiorrhiza*[J]. Journal of Experimental Botany, 2021, 72(13): 4915-4929.

[61] Li Y, Lu L, Wang Q, et al. Arbuscular mycorrhizal fungi promote nodulation and N2 fixation in soybean by specific root exudates[J]. Plant, Cell & Environment, 2025, 48(7): 5514-5528.

[62] Lu Z, Zou H, Cui J, et al. The *Rhus chinensis* genome provides insights into tannin, flavonoid biosynthesis, and glandular trichome development[J]. Plant Biotechnology Journal, 2026, 24(3): 988-1013.

[63] Tuo X, Hou L, Zhang Z, et al. Integrated physiological and transcriptomic analysis uncovers MYB-mediated regulation of the key biosynthetic gene PePAL1 driving postharvest lignification in *Pleurotus eryngii*[J]. Postharvest Biology and Technology, 2026, 240: 114422.

Fig. 1. Total polyphenol content, antioxidant capacities, and correlation heatmap of different samples. (A) TPC: Total polyphenol content (mg/g FW). Different letters indicate significant differences ($P < 0.05$).(B) ABTS: ABTS radical scavenging capacity (umol Trolox/g Fw).(C) DPPH: DPPH radical scavenging capacity (umol umol Trolox/g Fw).(D) FRAP: Ferric reducing antioxidant power (Fe^{2+}/g FW).(E) Correlation heatmap: Pearson correlation coefficients among TPC, ABTS, DPPH, and FRAP. Asterisks denote statistical significance (* $P < 0.05$, ** $P < 0.01$). The color scale from light yellow to dark green represents correlation coefficients from 0.90 to 1.00, indicating extremely strong positive correlations.

Fig. 2. Analysis of the metabolite composition and classification at different developmental stages of *Rubus chingii*. (A) Principal component analysis (PCA) plot of metabolites, where samples are color-coded by developmental stage (Green, Yellow, Orange, Pink, Red) or specific treatment groups (e.g., GR1-3, YE1-3, OR1-3, RE1-3, PI1-3). The plot displays clustering along PC1 (38.66% variance) and PC2 (19.63% variance), with shaded ellipses indicating significant groupings. (B) Classification of 1064 detected metabolites into Class I and Class II, visualized via donut charts. Class I is dominated by Flavonoids (48.9%), while Class II comprises Flavonols (29.7%) and other subclasses such as Flavones, Chalcones, and Lignans. (C) Stacked bar chart showing the number of metabolites across five developmental stages (Green, Yellow, Orange, Pink, Red). Each bar segment represents a specific chemical class (e.g., Flavonols, Flavones, Lignans, Tannins) as detailed in the legend, illustrating the compositional changes during development.

Fig. 3. Characterization of differentially accumulated metabolites (DAMs), correlation between co-expression modules and physiological indicators, and identification of key metabolites. (A) Number of differentially accumulated metabolites (DAMs) among the developmental stages. (B) Stacked bar chart illustrating the composition of the DAMs. (C) Correlation analysis between the co-expression modules and physiological indicators. (D) Classification of the metabolites within the turquoise module. (E) Classification of the DAMs within the

turquoise module. (F) Correlation network between the physiological indicators and key metabolites. (G) Classification of the key metabolites.

Fig. 4. Network pharmacological analysis of key metabolites and their targets: metabolite-target network, protein-protein interaction (PPI) network, and functional enrichment (KEGG and GO) analysis. (A) Key metabolite-target network. A comprehensive network illustrating the interactions between key metabolites (represented by green central nodes, e.g., pmp000046, grme02127) and their corresponding OD-related targets (represented by pink peripheral nodes). The network highlights the multi-target and multi-pathway synergistic regulatory mechanism of the core metabolites. (B) Protein-protein interaction (PPI) network of the targets. A complex interaction network of target proteins, where the node color intensity indicates the degree of connectivity (ranging from low/light pink to high/dark magenta, as shown in the gradient scale). Central hub targets with the highest degrees (e.g., AKT1, SRC, PIK3CA) are key regulators in the biological network. (C) KEGG pathway enrichment analysis of all targets. A bubble chart displaying the top significantly enriched KEGG pathways. The y-axis lists the pathway names, and the x-axis represents the enrichment score. The size of each bubble represents the number of enriched genes (count), and the color gradient from green to red represents the statistical significance. (D) Gene Ontology (GO) enrichment analysis of all targets. A categorized bubble chart showing the top enriched GO terms divided into molecular function (MF), biological process (BP), and cellular component (CC). Bubble size corresponds to the gene count, and color intensity indicates significance. Key enriched terms include "protein kinase activity" (MF), "response to hormone" and "negative regulation of apoptotic process" (BP), and "perinuclear region of cytoplasm" (CC).

Fig. 5. Molecular docking analysis of key metabolites and targets: binding energy heatmap and 3D binding mode visualization. (A) Heatmap of molecular docking binding energies between metabolites and targets. (B) 3D visualization of the metabolite-target binding sites.

Fig. 6. Transcriptomic dynamics, differential gene expression, pathway enrichment, and co-expression module correlation with physiological indicators across developmental stages. (A) Principal component analysis (PCA) plot of the transcriptomic data. (B) Number of differentially expressed genes (DEGs) among the developmental stages. (C) Heatmap of KEGG pathway enrichment analysis for the DEGs. (D) Correlation analysis between the co-expression modules and physiological indicators.

Fig. 7. Transcriptional and metabolic regulatory network of the phenylpropanoid pathway and the 'TF-RcPAL-polyphenol' cascade during fruit development. (A) Schematic diagram of the key metabolites synthesized in the phenylpropanoid biosynthesis pathway. (B) Heatmap of *RcPAL* and *Rc4CL* expression levels. (C) Correlation heatmap between key transcription factors (TFs) and RcPAL/Rc4CL. (D) Sequence analysis of the 2,000 bp promoter region of the

RcPAL gene. (E) Construction of the "TF-*RcPAL*-polyphenol" cascade regulatory network. Asterisks in the correlation heatmap denote statistical significance (* $P < 0.05$, ** $P < 0.01$).

Fig. 8. Molecular and functional characterization of the *RcPAL* gene and its transcriptional regulators in raspberry fruit development and tobacco transformation. (A) Relative expression levels of *RcPAL* and three transcription factors across different stages. (B) Subcellular localization of RcPAL and the three transcription factors. (C) Phenotypes of *RcPAL*-overexpressing tobacco plants. (D) Total phenolic content (TPC) in wild-type (WT) and *RcPAL*-overexpressing tobacco plants. (E) Schematic diagrams of the vectors constructed for the dual-luciferase reporter assay. (F) Luminescence intensity of the infiltrated leaves. Stronger fluorescence signals indicate the activation of the promoter by the transcription factors. (G) Quantitative analysis of the relative LUC/REN activities. (H) Growth of yeast transformed with different vectors. The numbers 10^0, 10^{-1}, 10^{-2}, 10^{-3}, and 10^{-4} represent the dilution series of the yeast cultures. SD-UL indicates the synthetic dropout (SD) medium lacking uracil (URA) and leucine (LEU). Different letters indicate significant differences at $P < 0.05$.

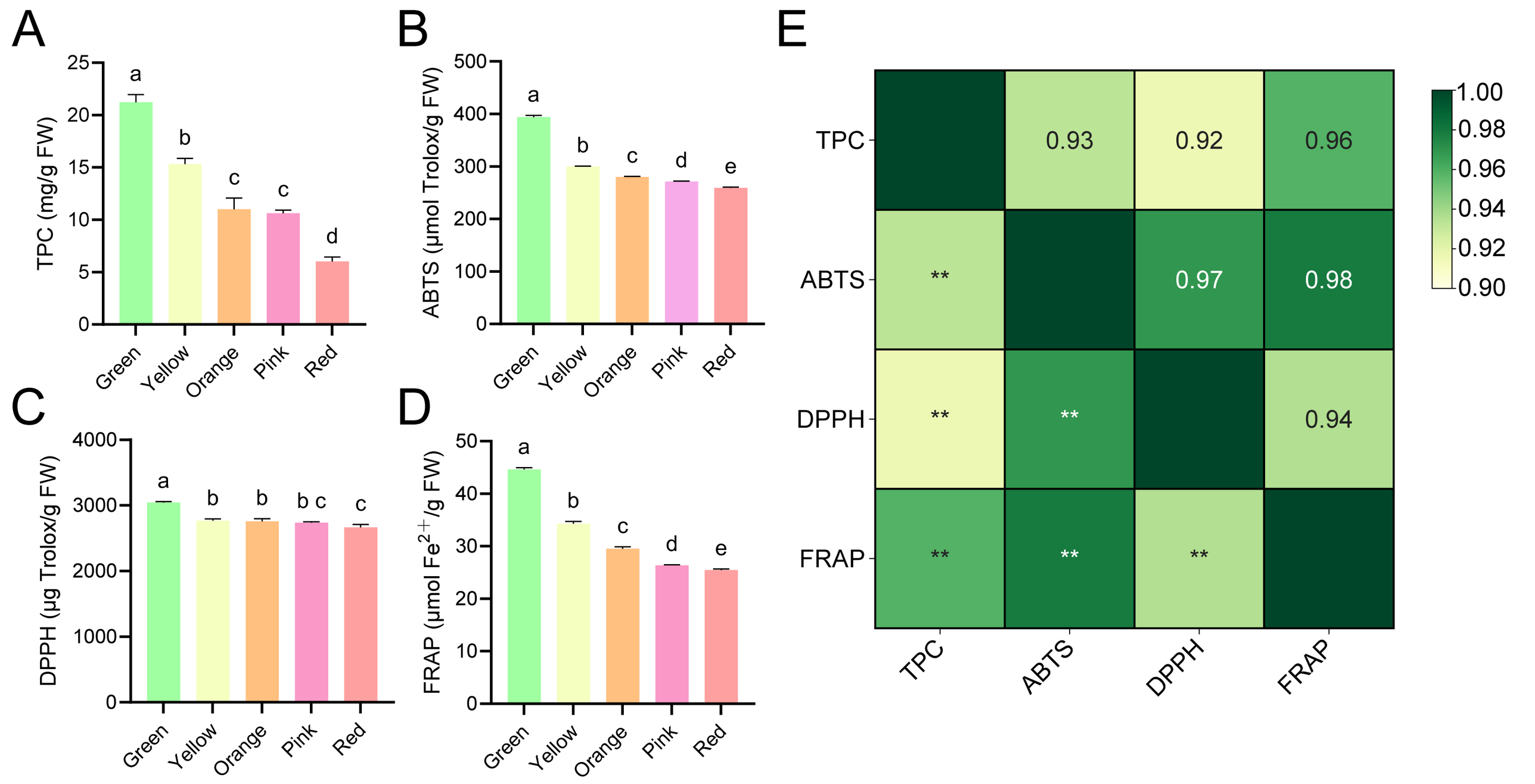
A
TPC (mg/g FW)
25
20
15
10
5
0
a
b
c
c
d
Green
Yellow
Orange
Pink
Red
B
ABTS (μmol Trolox/g FW)
500
400
300
200
100
0
a
b
c
d
e
Green
Yellow
Orange
Pink
Red
C
DPPH (μg Trolox/g FW)
4000
3000
2000
1000
0
a
b
b
b c
c
Green
Yellow
Orange
Pink
Red
D
FRAP (μmol Fe2+/g FW)
50
40
30
20
10
0
a
b
c
d
e
Green
Yellow
Orange
Pink
Red
E
TPC
ABTS
DPPH
FRAP
0.93
0.92
0.96
**
0.97
0.98
**
**
0.94
**
**
**
TPC
ABTS
DPPH
FRAP
1.00
0.98
0.96
0.94
0.92
0.90

A

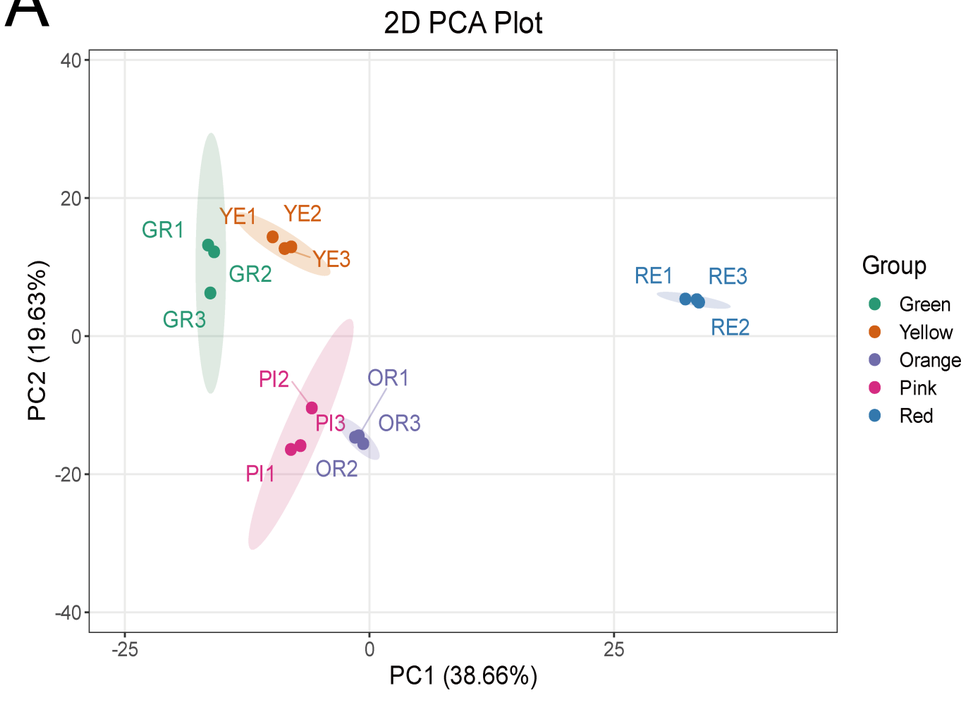
2D PCA Plot
PC2 (19.63%)
PC1 (38.66%)
40
20
0
-20
-40
-25
0
25
GR1
GR2
GR3
YE1
YE2
YE3
RE1
RE2
RE3
PI1
PI2
PI3
OR1
OR2
OR3
Group
Green
Yellow
Orange
Pink
Red

B

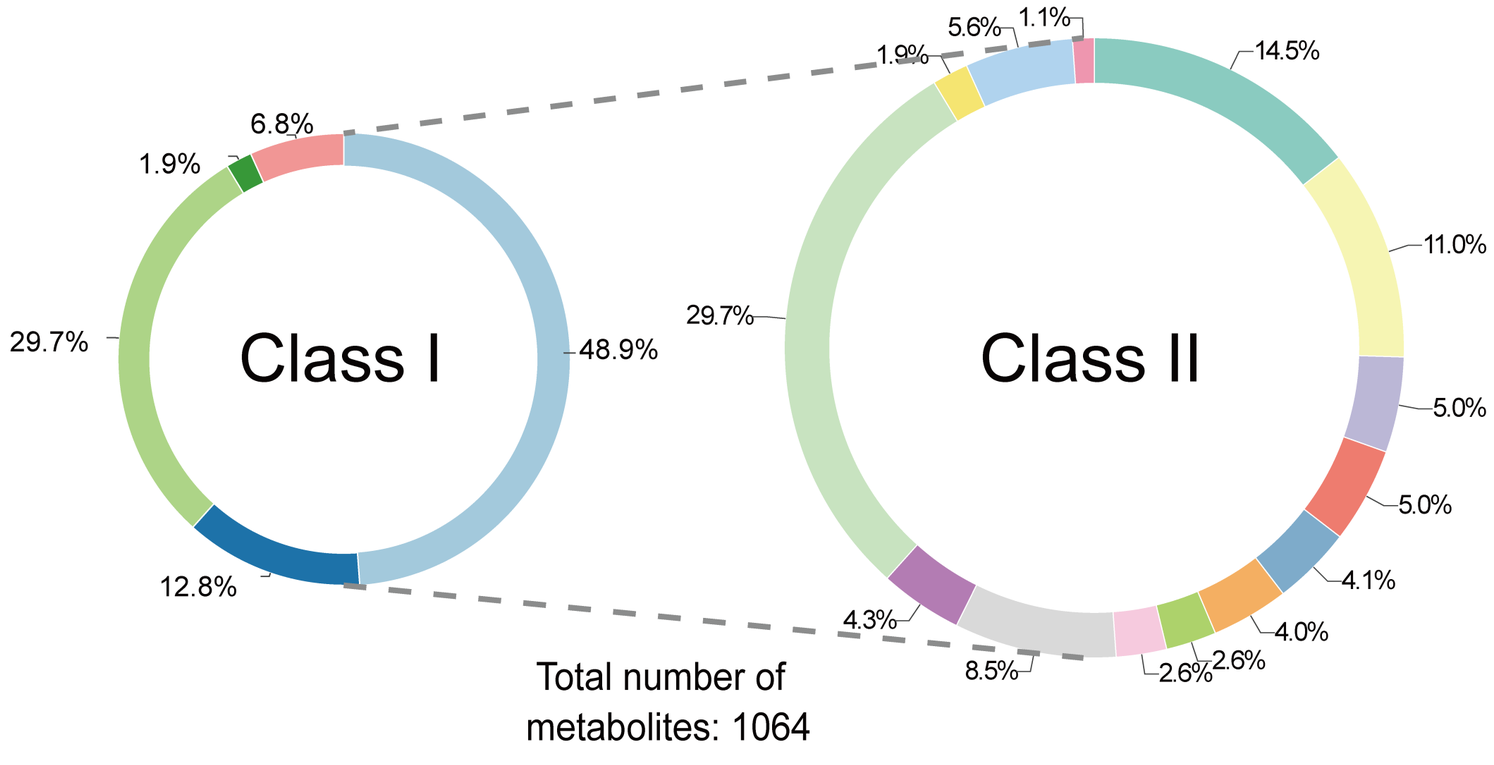
Class I
Class II
6.8%
1.9%
29.7%
48.9%
12.8%
1.9%
5.6%
1.1%
14.5%
29.7%
11.0%
5.0%
5.0%
4.1%
4.0%
2.6%
2.6%
8.5%
4.3%
Total number of
metabolites: 1064

C

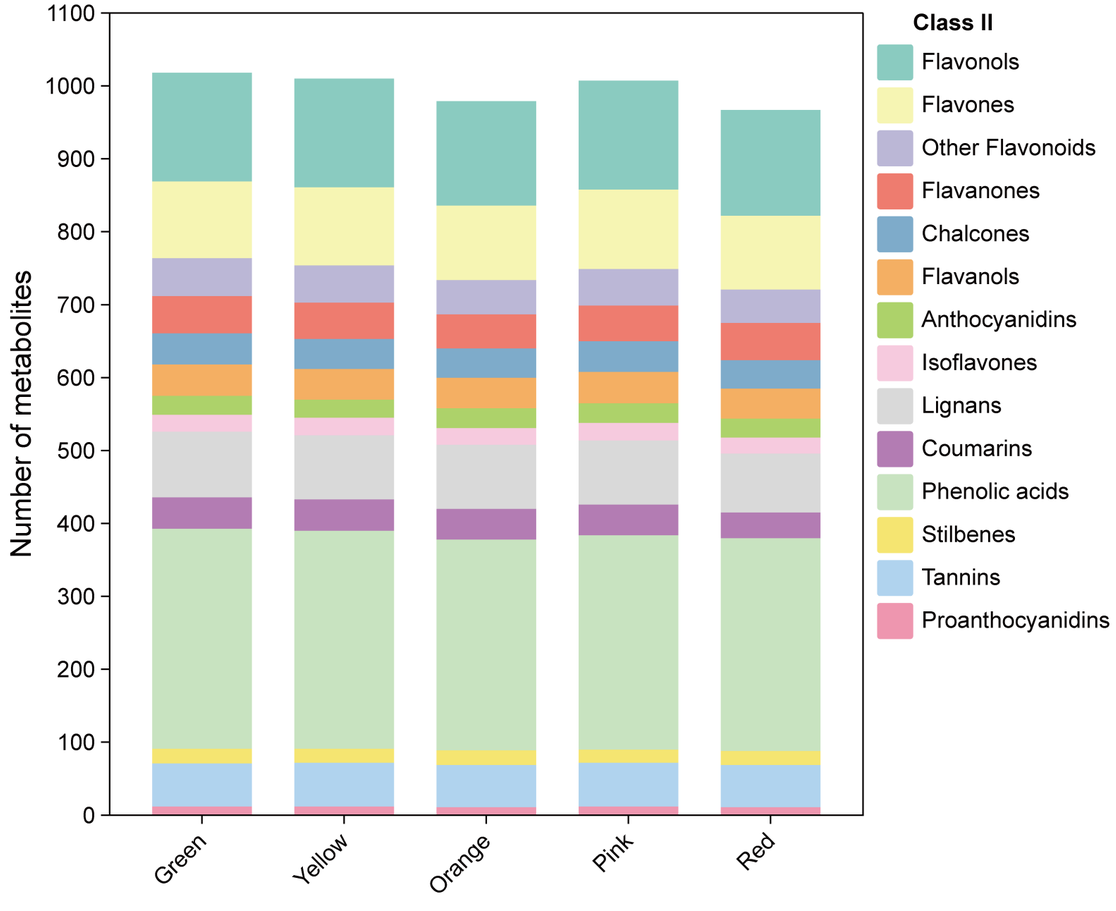
Number of metabolites
1100
1000
900
800
700
600
500
400
300
200
100
0
Green
Yellow
Orange
Pink
Red
Class II
Flavonols
Flavones
Other Flavonoids
Flavanones
Chalcones
Flavanols
Anthocyanidins
Isoflavones
Lignans
Coumarins
Phenolic acids
Stilbenes
Tannins
Proanthocyanidins

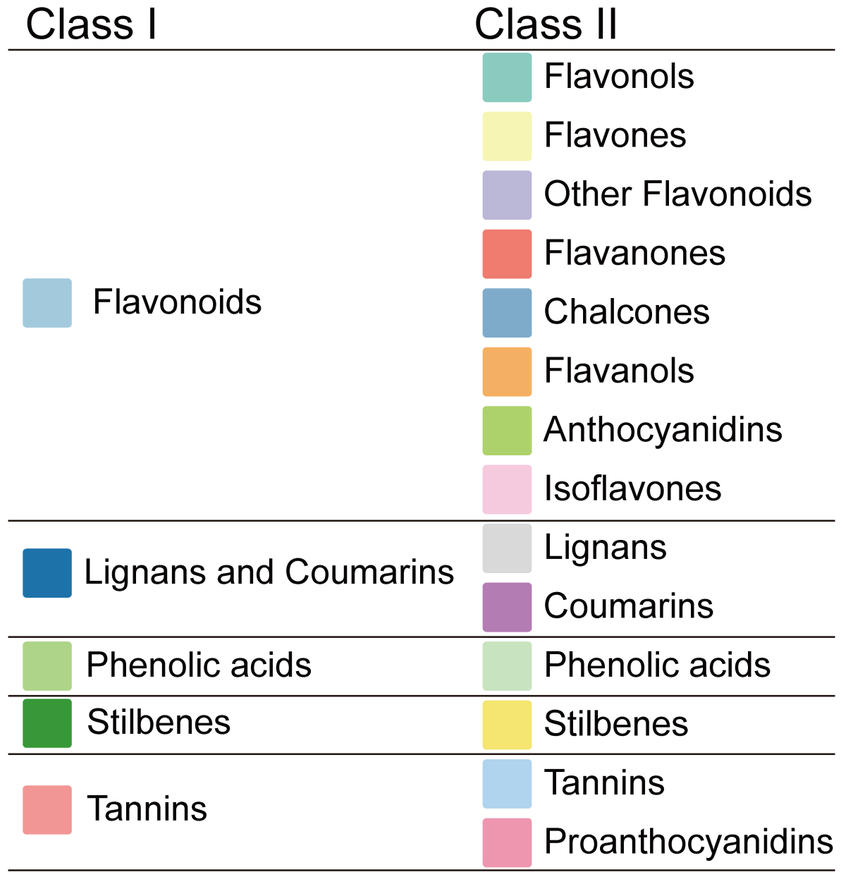
Class I
Class II
Flavonoids
Flavonols
Flavones
Other Flavonoids
Flavanones
Chalcones
Flavanols
Anthocyanidins
Isoflavones
Lignans and Coumarins
Lignans
Coumarins
Phenolic acids
Phenolic acids
Stilbenes
Stilbenes
Tannins
Tannins
Proanthocyanidins

A

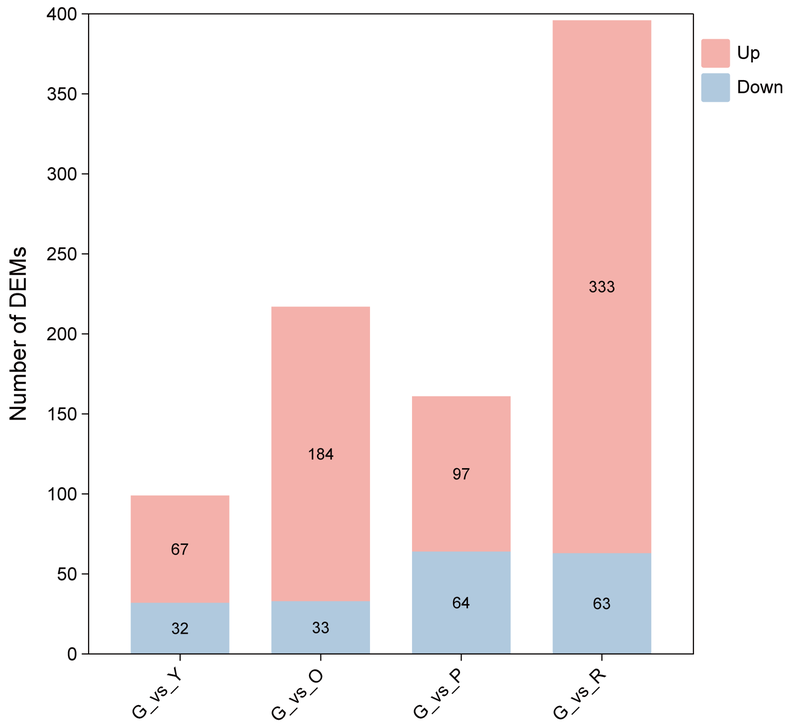
Number of DEMs
Up
Down
67
32
184
33
97
64
333
63
G_vs_Y
G_vs_O
G_vs_P
G_vs_R

B

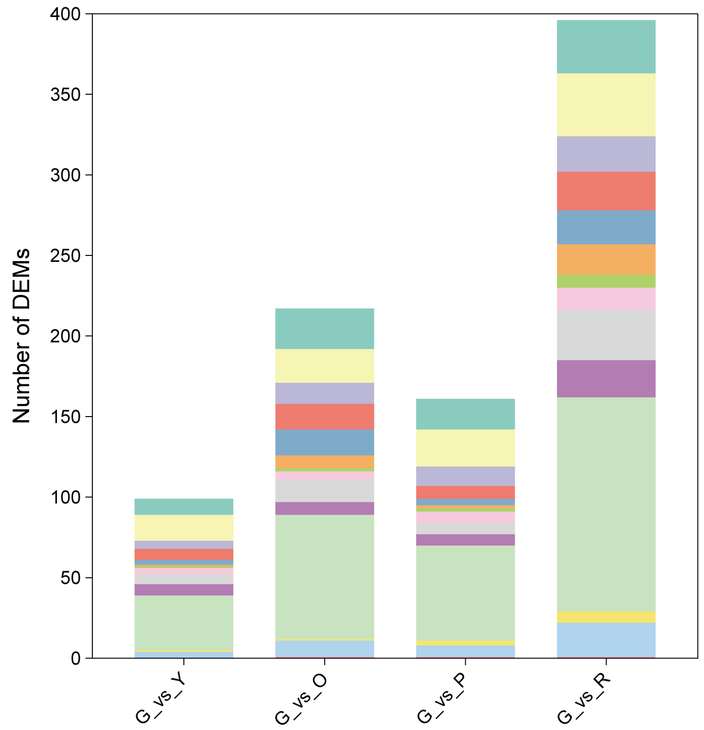
Number of DEMs
G_vs_Y
G_vs_O
G_vs_P
G_vs_R

C

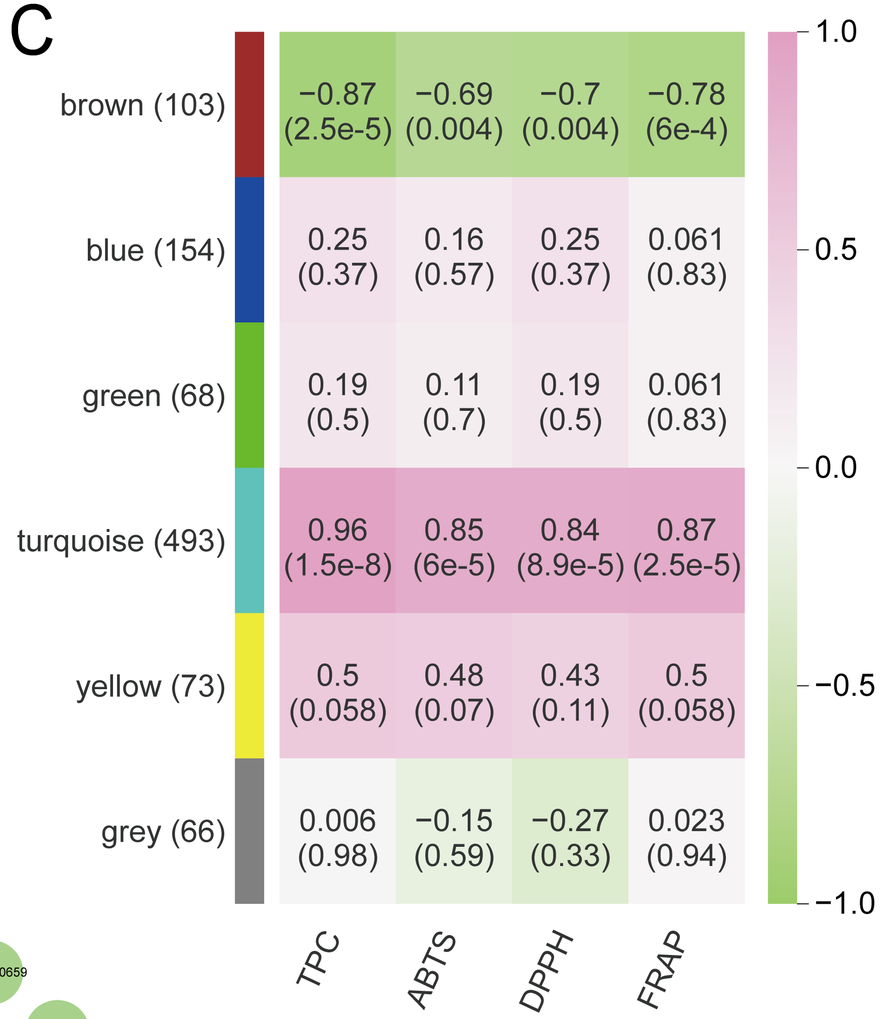
brown (103)
blue (154)
green (68)
turquoise (493)
yellow (73)
grey (66)
−0.87 (2.5e-5)
−0.69 (0.004)
−0.7 (0.004)
−0.78 (6e-4)
0.25 (0.37)
0.16 (0.57)
0.25 (0.37)
0.061 (0.83)
0.19 (0.5)
0.11 (0.7)
0.19 (0.5)
0.061 (0.83)
0.96 (1.5e-8)
0.85 (6e-5)
0.84 (8.9e-5)
0.87 (2.5e-5)
0.5 (0.058)
0.48 (0.07)
0.43 (0.11)
0.5 (0.058)
0.006 (0.98)
−0.15 (0.59)
−0.27 (0.33)
0.023 (0.94)
TPC
ABTS
DPPH
FRAP
1.0
0.5
0.0
−0.5
−1.0

D

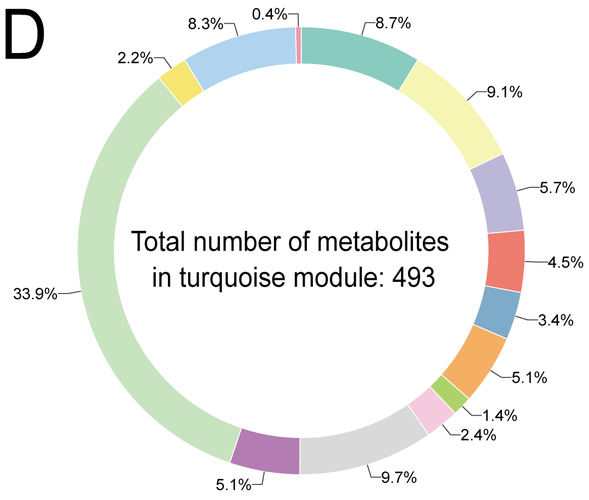
Total number of metabolites in turquoise module: 493
8.3%
0.4%
8.7%
2.2%
9.1%
5.7%
4.5%
33.9%
3.4%
5.1%
1.4%
2.4%
5.1%
9.7%


Class II
Flavonols
Flavones
Other Flavonoids
Flavanones
Chalcones
Flavanols
Anthocyanidins
Isoflavones
Lignans
Coumarins
Phenolic acids
Stilbenes
Tannins
Proanthocyanidins

E

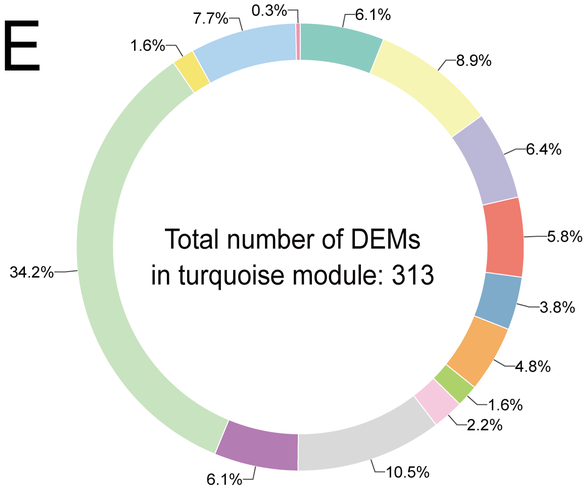
Total number of DEMs in turquoise module: 313
7.7%
0.3%
6.1%
1.6%
8.9%
6.4%
34.2%
5.8%
3.8%
4.8%
1.6%
2.2%
6.1%
10.5%

F

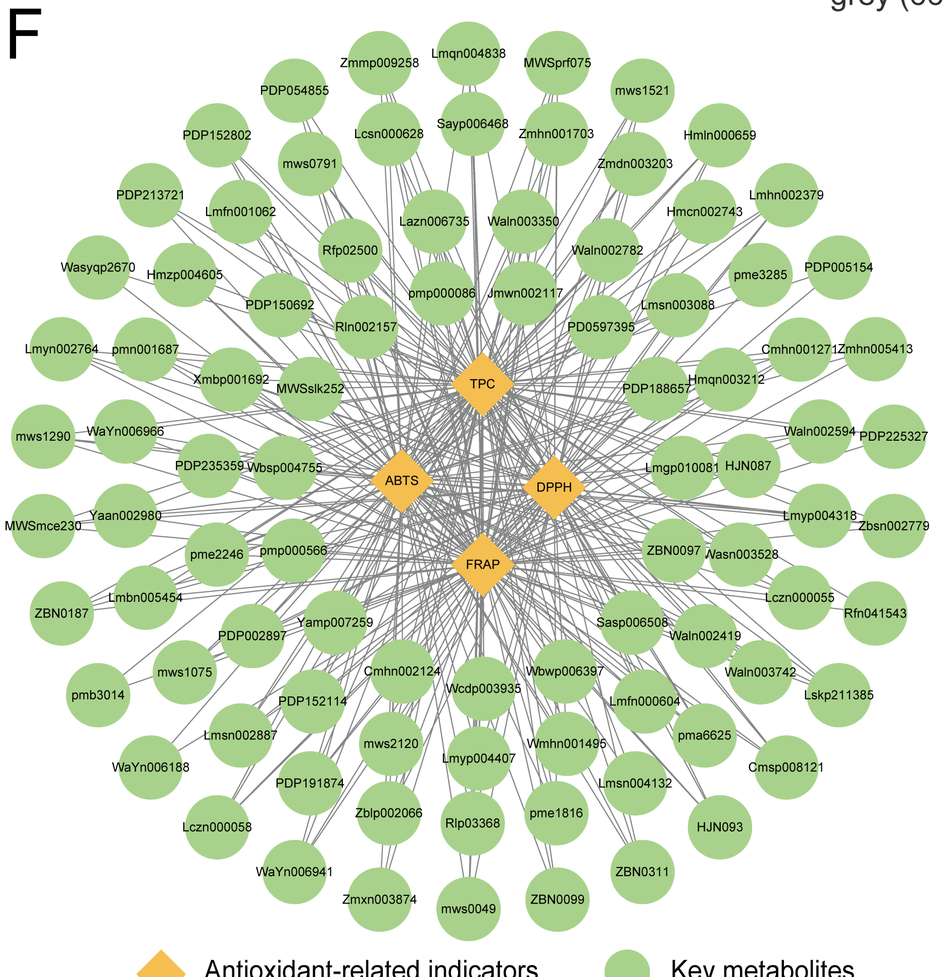
TPC
ABTS
DPPH
FRAP
Antioxidant-related indicators
Key metabolites

G

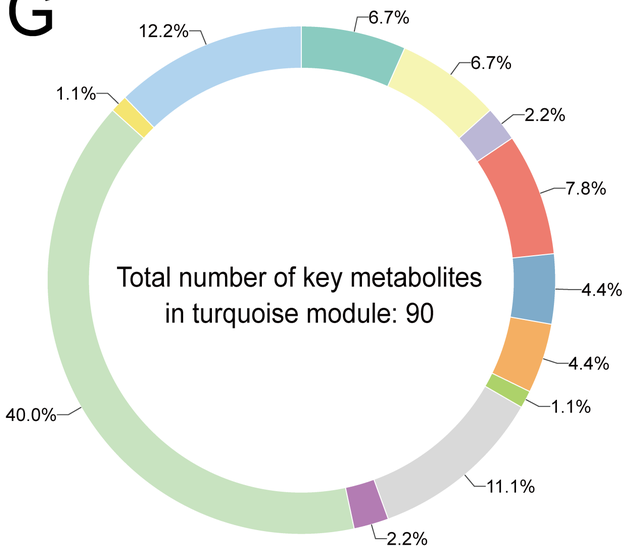
Total number of key metabolites in turquoise module: 90
12.2%
6.7%
1.1%
6.7%
2.2%
7.8%
4.4%
4.4%
40.0%
1.1%
11.1%
2.2%

A

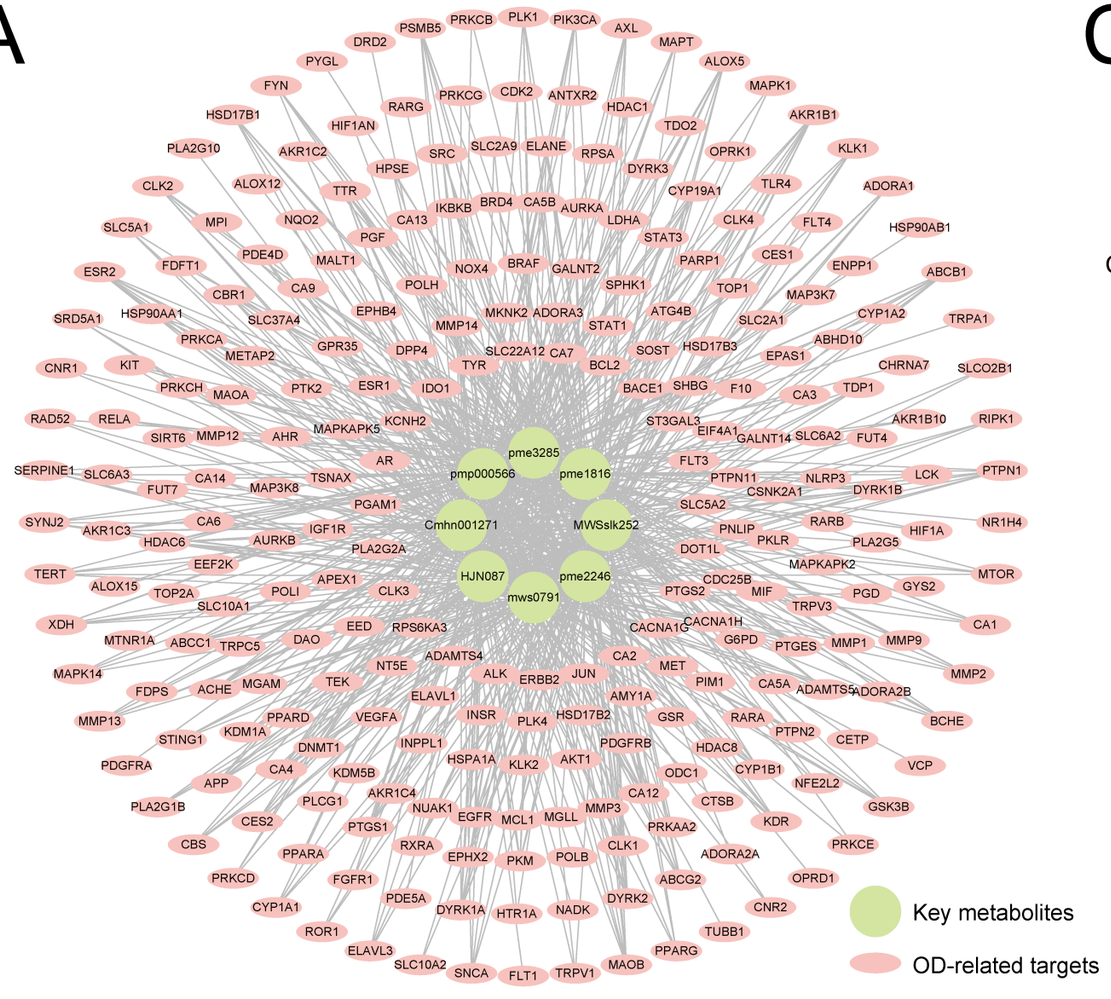
pme3285
pmp000566
pme1816
Cmhn001271
MWSslk252
HJN087
pme2246
mws0791
Key metabolites
OD-related targets

B

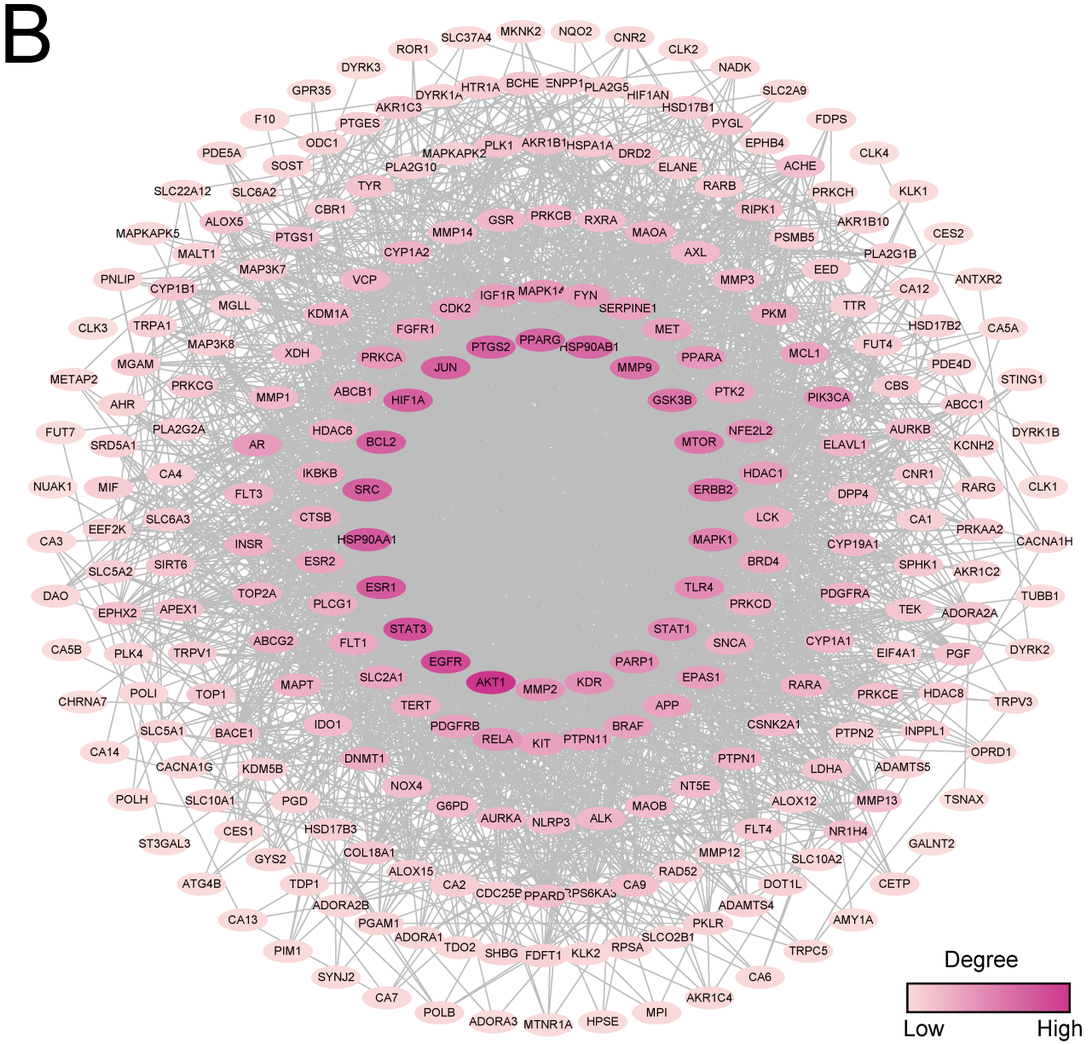
Degree
Low
High

C

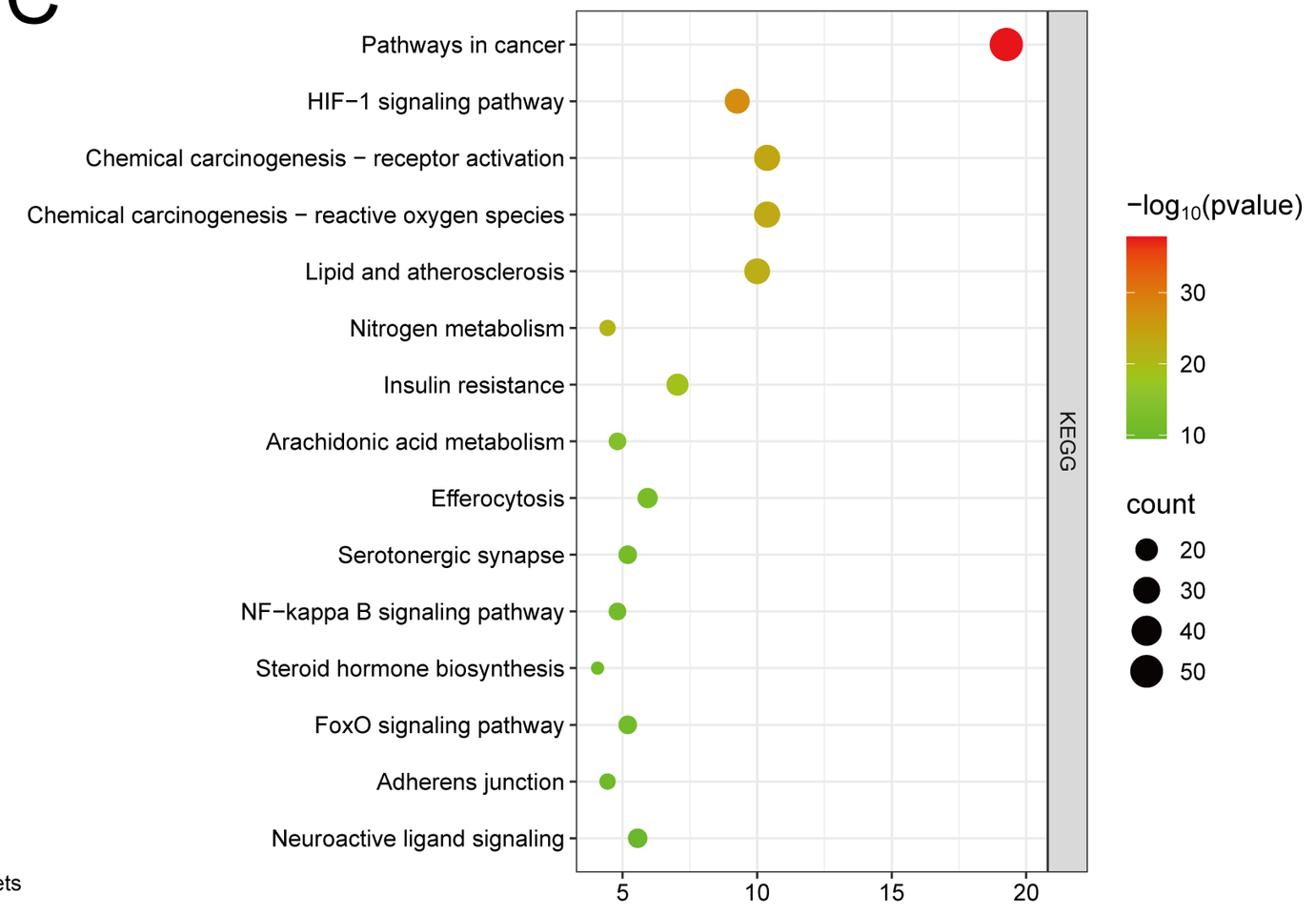
Pathways in cancer
HIF−1 signaling pathway
Chemical carcinogenesis − receptor activation
Chemical carcinogenesis − reactive oxygen species
Lipid and atherosclerosis
Nitrogen metabolism
Insulin resistance
Arachidonic acid metabolism
Efferocytosis
Serotonergic synapse
NF−kappa B signaling pathway
Steroid hormone biosynthesis
FoxO signaling pathway
Adherens junction
Neuroactive ligand signaling
KEGG
5
10
15
20
−log10(pvalue)
30
20
10
count
20
30
40
50

D

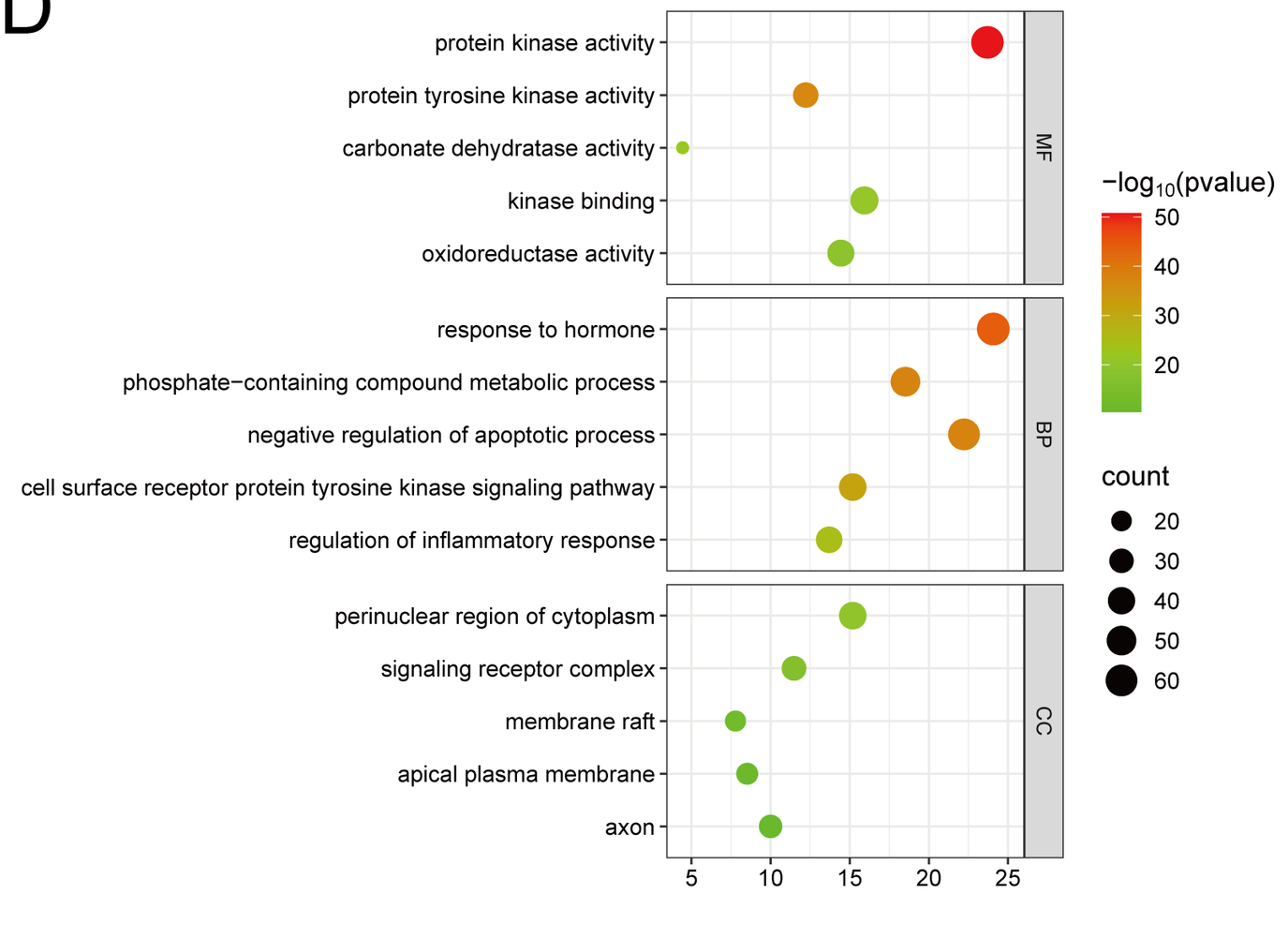
protein kinase activity
protein tyrosine kinase activity
carbonate dehydratase activity
kinase binding
oxidoreductase activity
MF
response to hormone
phosphate−containing compound metabolic process
negative regulation of apoptotic process
cell surface receptor protein tyrosine kinase signaling pathway
regulation of inflammatory response
BP
perinuclear region of cytoplasm
signaling receptor complex
membrane raft
apical plasma membrane
axon
CC
5
10
15
20
25
−log10(pvalue)
50
40
30
20
count
20
30
40
50
60

A

Cmhn001271	pme2246	HJN087	mws0791	MWSslk252	pme3285	pmp000566	pme1816	
-7.00	-6.40	-10.40	-11.00	-10.50	-6.00	-6.10	-6.10	AKT1
-7.30	-8.70	-7.80	-9.80	-10.20	-8.30	-8.70	-8.30	EGFR
-8.40	-8.20	-8.10	-8.20	-8.60	-7.20	-7.20	-7.40	STAT3
-8.80	-8.80	-8.70	-8.10	-8.70	-7.20	-6.30	-8.20	ESR1
-8.30	-7.90	-7.70	-9.20	-7.70	-7.00	-7.30	-7.90	HSP90AA1
-8.60	-7.70	-7.60	-7.80	-8.00	-6.60	-8.10	-7.30	HIF1A
-9.10	-8.20	-8.50	-9.60	-9.90	-7.30	-7.30	-7.40	BCL2
-8.00	-7.80	-9.30	-9.80	-7.50	-7.90	-7.10	-8.30	SRC
-8.80	-7.50	-8.30	-8.60	-9.80	-7.90	-7.50	-7.60	JUN
-9.70	-9.10	-9.70	-7.90	-7.10	-9.00	-9.10	-9.70	PTGS2

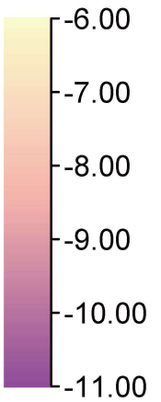

B

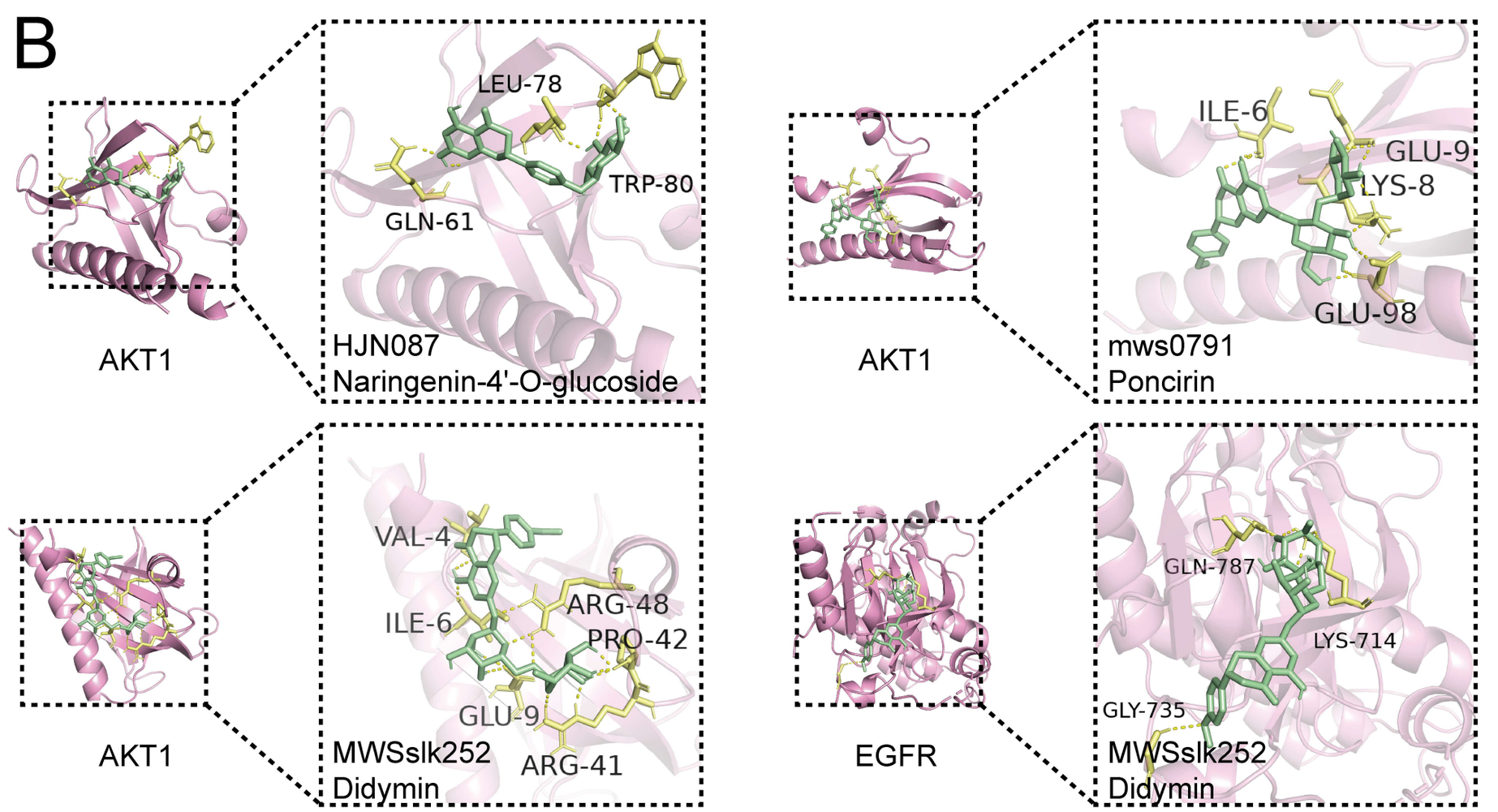

A

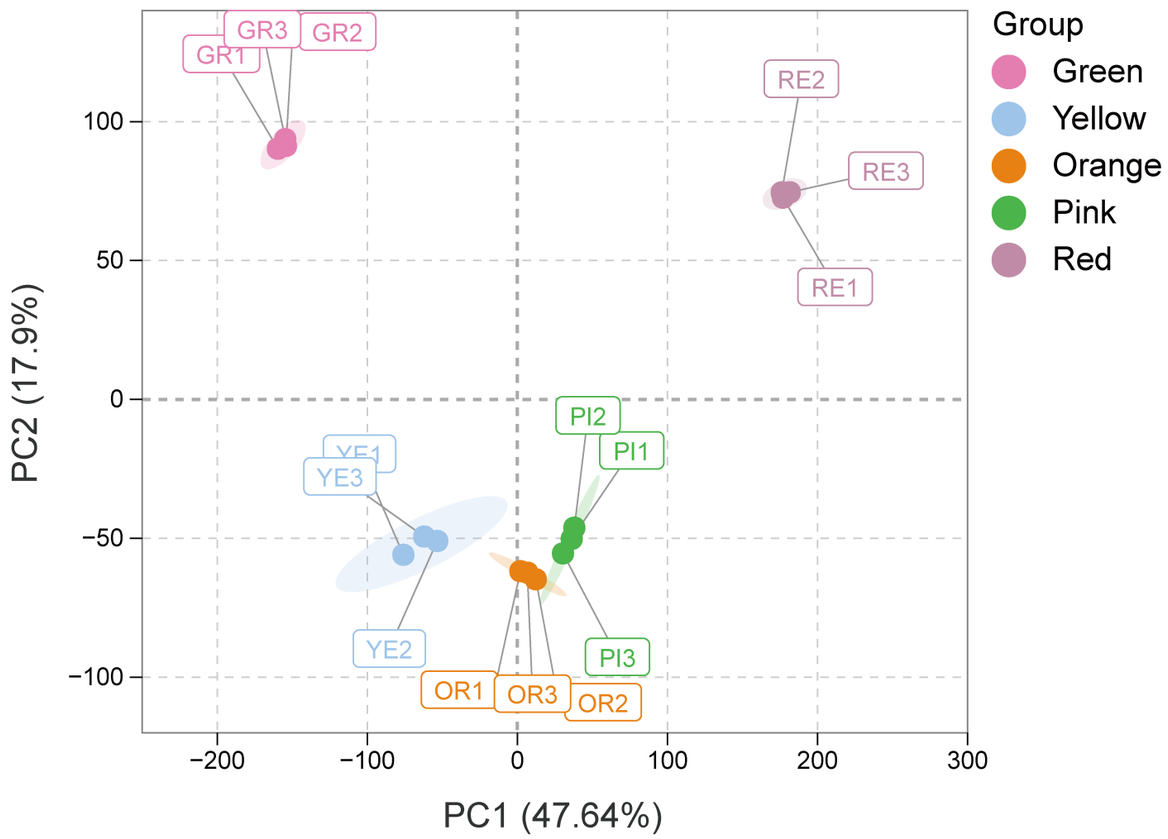
GR3
GR2
GR1
RE2
RE3
RE1
PI2
PI1
YE3
YE2
PI3
OR1
OR3
OR2
100
50
0
−50
−100
−200
−100
0
100
200
300
PC2 (17.9%)
PC1 (47.64%)
Group
Green
Yellow
Orange
Pink
Red

B

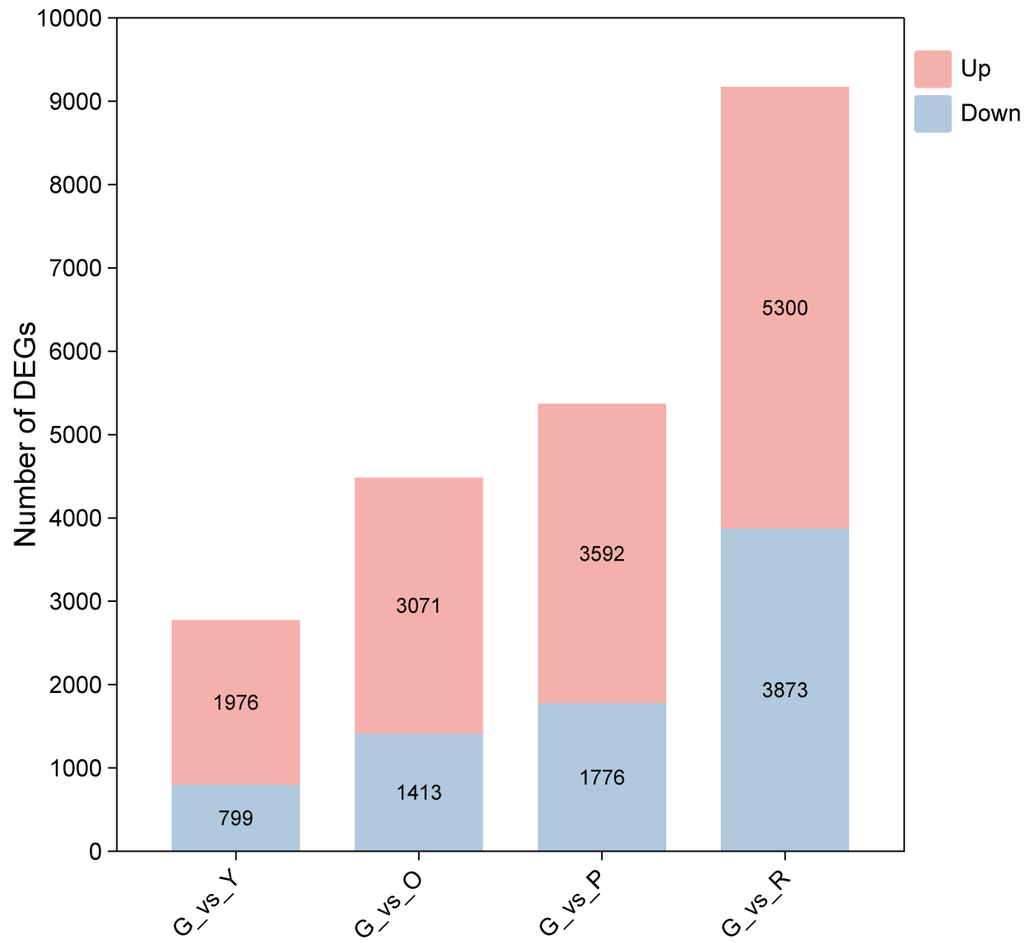
10000
9000
8000
7000
6000
5000
4000
3000
2000
1000
0
Number of DEGs
Up
Down
1976
799
3071
1413
3592
1776
5300
3873
G_vs_Y
G_vs_O
G_vs_P
G_vs_R

C

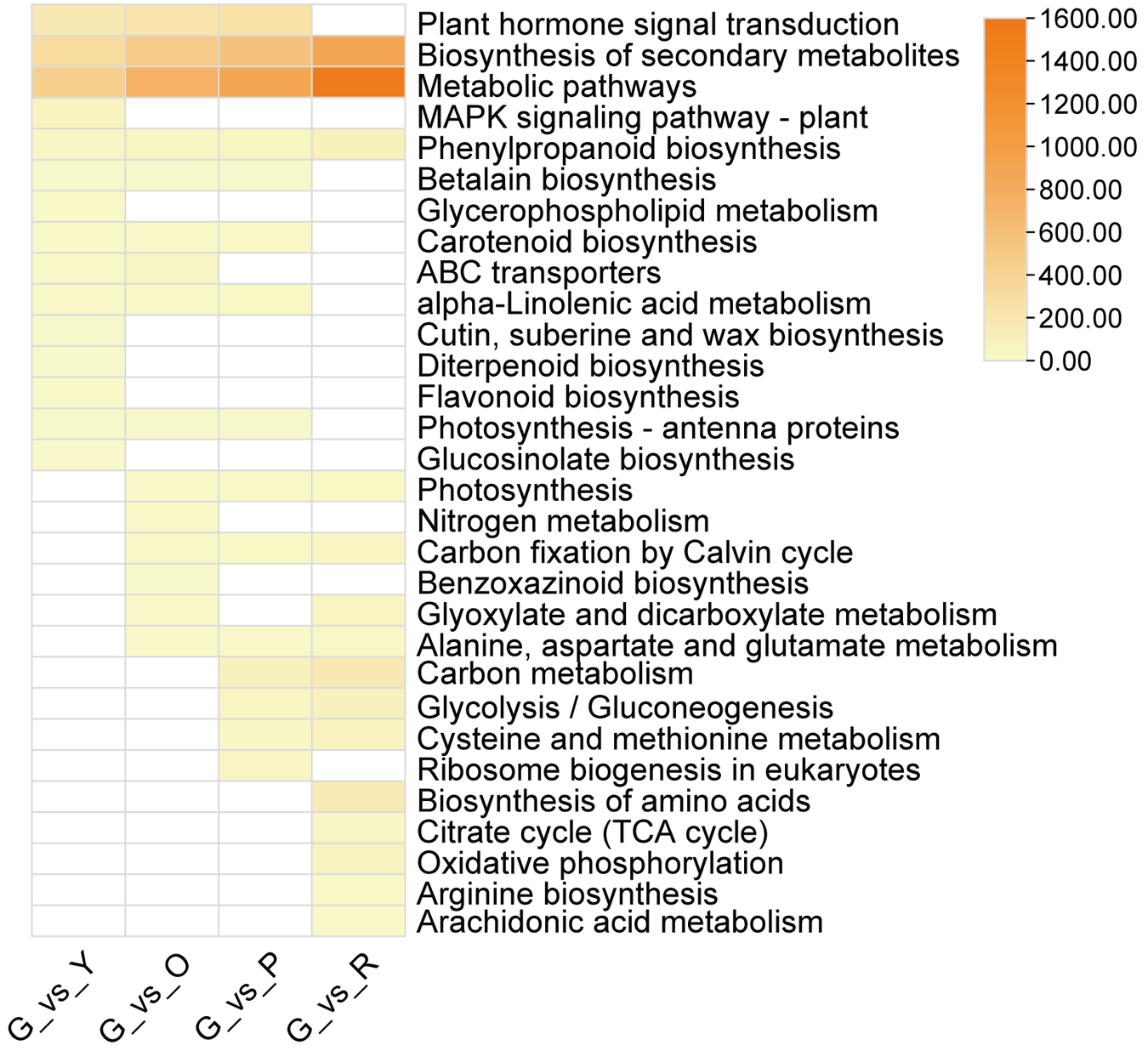
Plant hormone signal transduction
Biosynthesis of secondary metabolites
Metabolic pathways
MAPK signaling pathway - plant
Phenylpropanoid biosynthesis
Betalain biosynthesis
Glycerophospholipid metabolism
Carotenoid biosynthesis
ABC transporters
alpha-Linolenic acid metabolism
Cutin, suberine and wax biosynthesis
Diterpenoid biosynthesis
Flavonoid biosynthesis
Photosynthesis - antenna proteins
Glucosinolate biosynthesis
Photosynthesis
Nitrogen metabolism
Carbon fixation by Calvin cycle
Benzoxazinoid biosynthesis
Glyoxylate and dicarboxylate metabolism
Alanine, aspartate and glutamate metabolism
Carbon metabolism
Glycolysis / Gluconeogenesis
Cysteine and methionine metabolism
Ribosome biogenesis in eukaryotes
Biosynthesis of amino acids
Citrate cycle (TCA cycle)
Oxidative phosphorylation
Arginine biosynthesis
Arachidonic acid metabolism
1600.00
1400.00
1200.00
1000.00
800.00
600.00
400.00
200.00
0.00
G_vs_Y
G_vs_O
G_vs_P
G_vs_R

D

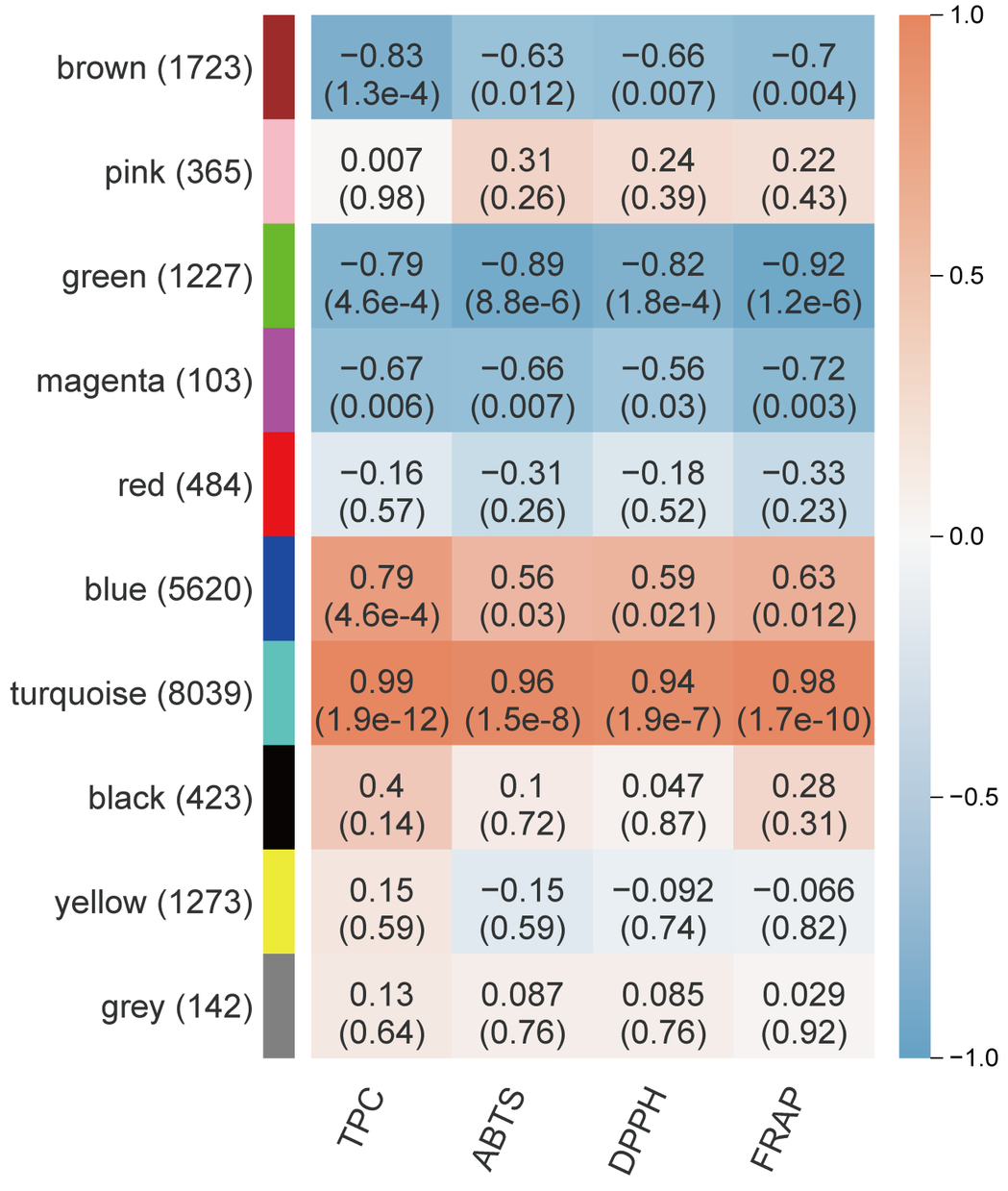
brown (1723)
−0.83 (1.3e-4)
−0.63 (0.012)
−0.66 (0.007)
−0.7 (0.004)
pink (365)
0.007 (0.98)
0.31 (0.26)
0.24 (0.39)
0.22 (0.43)
green (1227)
−0.79 (4.6e-4)
−0.89 (8.8e-6)
−0.82 (1.8e-4)
−0.92 (1.2e-6)
magenta (103)
−0.67 (0.006)
−0.66 (0.007)
−0.56 (0.03)
−0.72 (0.003)
red (484)
−0.16 (0.57)
−0.31 (0.26)
−0.18 (0.52)
−0.33 (0.23)
blue (5620)
0.79 (4.6e-4)
0.56 (0.03)
0.59 (0.021)
0.63 (0.012)
turquoise (8039)
0.99 (1.9e-12)
0.96 (1.5e-8)
0.94 (1.9e-7)
0.98 (1.7e-10)
black (423)
0.4 (0.14)
0.1 (0.72)
0.047 (0.87)
0.28 (0.31)
yellow (1273)
0.15 (0.59)
−0.15 (0.59)
−0.092 (0.74)
−0.066 (0.82)
grey (142)
0.13 (0.64)
0.087 (0.76)
0.085 (0.76)
0.029 (0.92)
TPC
ABTS
DPPH
FRAP
1.0
0.5
0.0
−0.5
−1.0

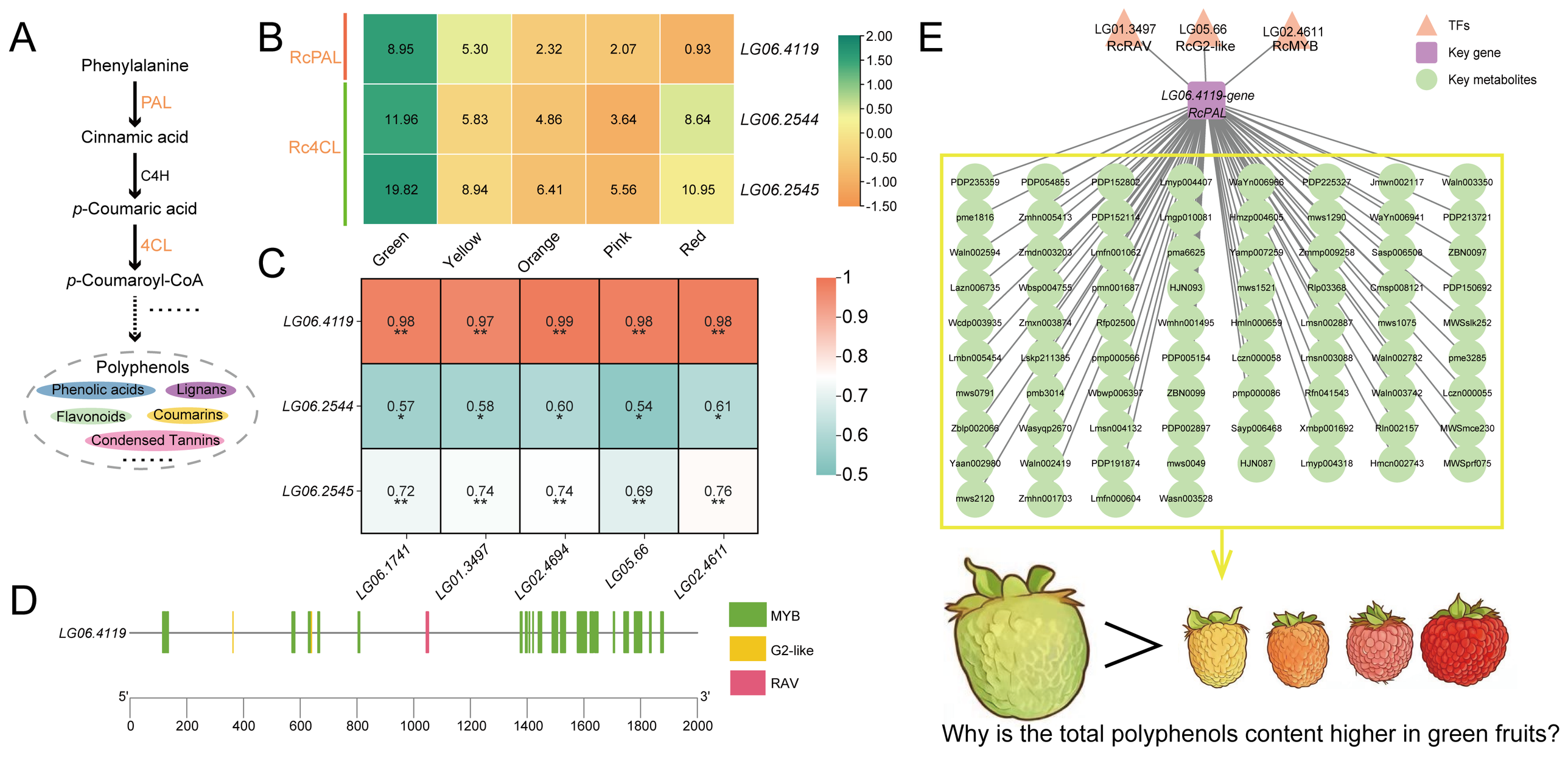
A
Phenylalanine
PAL
Cinnamic acid
C4H
p-Coumaric acid
4CL
p-Coumaroyl-CoA
Polyphenols
Phenolic acids
Lignans
Flavonoids
Coumarins
Condensed Tannins
B
RcPAL
Rc4CL
8.95
5.30
2.32
2.07
0.93
LG06.4119
11.96
5.83
4.86
3.64
8.64
LG06.2544
19.82
8.94
6.41
5.56
10.95
LG06.2545
2.00
1.50
1.00
0.50
0.00
-0.50
-1.00
-1.50
Green
Yellow
Orange
Pink
Red
C
LG06.4119
LG06.2544
LG06.2545
0.98 **
0.97 **
0.99 **
0.98 **
0.98 **
0.57 *
0.58 *
0.60 *
0.54 *
0.61 *
0.72 **
0.74 **
0.74 **
0.69 **
0.76 **
1
0.9
0.8
0.7
0.6
0.5
LG06.1741
LG01.3497
LG02.4694
LG05.66
LG02.4611
D
LG06.4119
5'
3'
0
200
400
600
800
1000
1200
1400
1600
1800
2000
MYB
G2-like
RAV
E
LG01.3497
RcRAV
LG05.66
RcG2-like
LG02.4611
RcMYB
TFs
Key gene
Key metabolites
LG06.4119-gene
RcPAL
PDP235359
PDP054855
PDP152802
Lmyp004407
WaYn006966
PDP225327
Jmwn002117
Waln003350
pme1816
Zmhn005413
PDP152114
Lmgp010081
Hmzp004605
mws1290
WaYn006941
PDP213721
Waln002594
Zmdn003203
Lmfn001062
pma6625
Yamp007259
Zmmp009258
Sasp006508
ZBN0097
Lazn006735
Wbsp004755
pmn001687
HJN093
mws1521
Rlp03368
Cmsp008121
PDP150692
Wcdp003935
Zmxn003874
Rfp02500
Wmhn001495
Hmln000659
Lmsn002887
mws1075
MWSslk252
Lmbn005454
Lskp211385
pmp000566
PDP005154
Lczn000058
Lmsn003088
Waln002782
pme3285
mws0791
pmb3014
Wbwp006397
ZBN0099
pmp000086
Rfn041543
Waln003742
Lczn000055
Zblp002066
Wasyqp2670
Lmsn004132
PDP002897
Sayp006468
Xmbp001692
Rln002157
MWSmce230
Yaan002980
Waln002419
PDP191874
mws0049
HJN087
Lmyp004318
Hmcn002743
MWSprf075
mws2120
Zmhn001703
Lmfn000604
Wasn003528
Why is the total polyphenols content higher in green fruits?

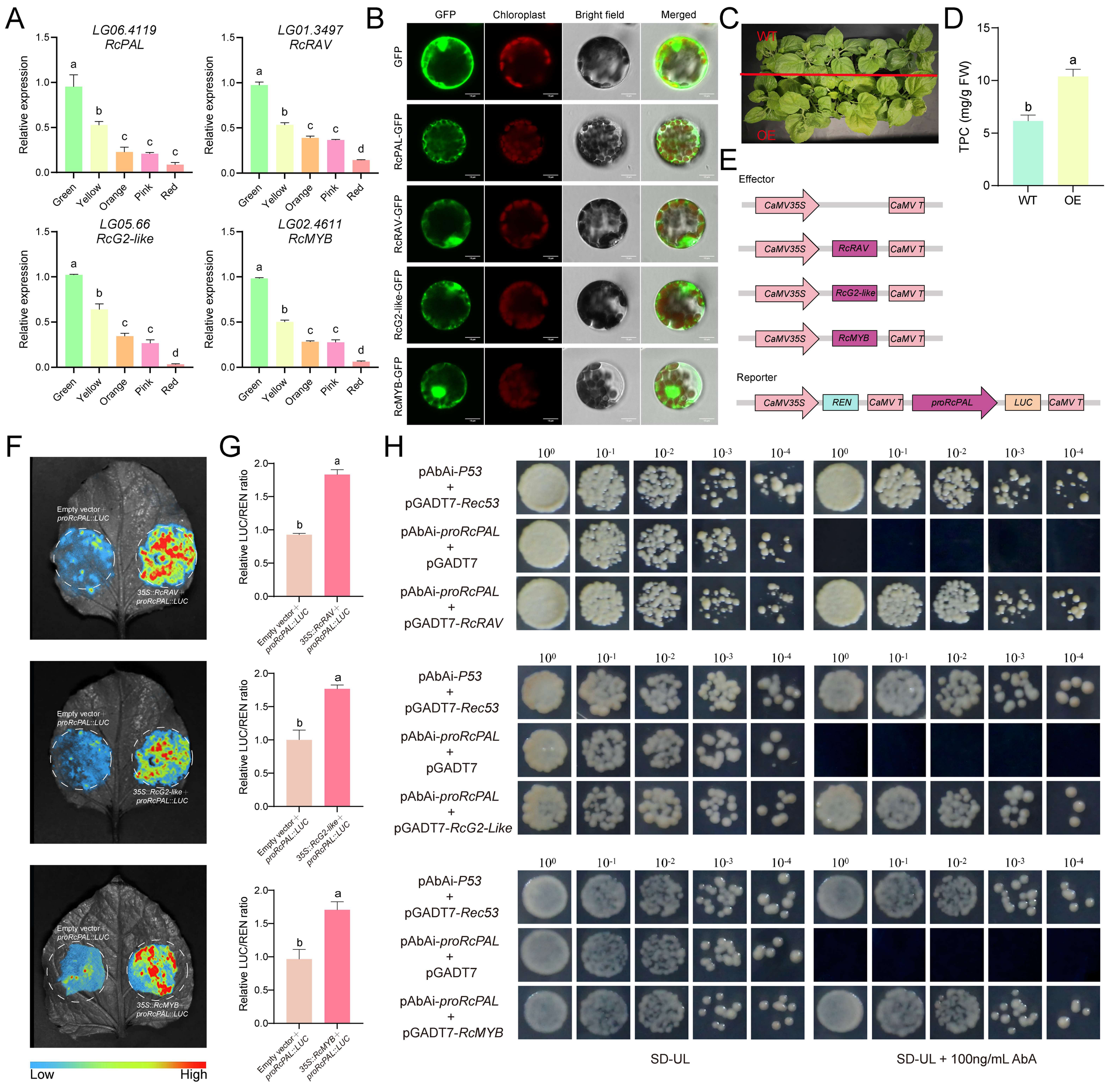

A
LG06.4119
RcPAL
LG01.3497
RcRAV
LG05.66
RcG2-like
LG02.4611
RcMYB
Relative expression
Green
Yellow
Orange
Pink
Red
B
GFP
Chloroplast
Bright field
Merged
GFP
RcPAL-GFP
RcRAV-GFP
RcG2-like-GFP
RcMYB-GFP
C
WT
OE
D
TPC (mg/g FW)
WT
OE
E
Effector
CaMV35S
CaMV T
RcRAV
RcG2-like
RcMYB
Reporter
REN
proRcPAL
LUC
F
Empty vector+
proRcPAL::LUC
35S::RcRAV+
proRcPAL::LUC
35S::RcG2-like+
proRcPAL::LUC
35S::RcMYB+
proRcPAL::LUC
Low
High
G
Relative LUC/REN ratio
Empty vector+
proRcPAL::LUC
35S::RcRAV+
proRcPAL::LUC
35S::RcG2-like+
proRcPAL::LUC
35S::RcMYB+
proRcPAL::LUC
H
pAbAi-P53
+
pGADT7-Rec53
pAbAi-proRcPAL
+
pGADT7
pAbAi-proRcPAL
+
pGADT7-RcRAV
pAbAi-proRcPAL
+
pGADT7-RcG2-Like
pAbAi-proRcPAL
+
pGADT7-RcMYB
SD-UL
SD-UL + 100ng/mL AbA

Supplementary Files

This is a list of supplementary files associated with this preprint. Click to download.

- SupplementaryTable.xlsx